Dual binding motifs underpin the hierarchical association of perilipins1–3 with lipid droplets

Dalila Ajjaji, Kalthoum Ben M'Barek, Michael L Mimmack, Cheryl England, Haya Herscovitz, Liang Dong, Richard G Kay, Satish Patel, Vladimir Saudek, Donald M Small, et al.

Dual binding motifs underpin the hierarchical association of perilipins1-3 with lipid droplets.

Dalila Ajjaji[1,*], Kalthoum Ben Mbarek[1,*], Michael L. Mimmack[2], Cheryl England[3], Haya Herscovitz[3], Liang Dong[2], Richard G. Kay[2], Satish Patel[2], Vladimir Saudek[2], Donald M. Small[3,‡], David B. Savage[2,‡] and Abdou Rachid Thiam[1,‡]

[1]Laboratoire de Physique Statistique, Ecole Normale Supérieure, PSL Research University, Sorbonne Université, UPMC Université Paris 06, Université Paris Diderot, CNRS, Paris, France

[2]University of Cambridge Metabolic Research Laboratories, Wellcome Trust-Medical Research Council Institute of Metabolic Science, Cambridge CB2 0QQ, United Kingdom

[3]Department of Physiology & Biophysics, Boston University School of Medicine, Boston, MA, USA

[*] equal contribution

[‡] corresponding authors

Correspondence to:

Prof. Donald M. Small,
Email: donmacfsmall@gmail.com

or
Prof. David B. Savage,
Email: dbs23@medschl.cam.ac.uk

or
Dr. Abdou Rachid Thiam,
Email: thiam@lps.ens.fr

Abstract

Lipid droplets (LDs) in all eukaryotic cells are coated with at least one of the perilipin family of proteins. They all regulate key intracellular lipases but do so to significantly different extents. Where more than one perilipin is expressed in a cell, they associate with LDs in a hierarchical manner. In vivo, this means that lipid flux control in a particular cell or tissue type is heavily influenced by the specific perilipins present on its LDs. Despite their early discovery, exactly how perilipins target LDs and why they displace each other in a 'hierarchical' manner remains unclear. They all share an amino-terminal 11-mer repeat amphipathic region suggested to be involved in LD targeting. Here, we show that in vivo this domain functions as a primary highly reversible LD targeting motif in perilipins1-3 and, in vitro, we document reversible and competitive binding between a wildtype purified perilipin1 11-mer repeat peptide and a mutant with reduced binding affinity to both 'naked' and phospholipid coated oil-water interfaces. We also present data suggesting that a second carboxy-terminal 4-helix bundle domain stabilizes LD binding in perilipin1 more effectively than in perilipin2, whereas in perilipin3 it weakens binding. These findings suggest that dual amphipathic helical regions mediate LD targeting and underpin the hierarchical binding of perilipins1-3 to LDs.

Introduction

Lipid droplets (LDs) form in almost all cell types and constitute the primary organelles for lipid storage. They consist of a neutral lipid core surrounded by an amphipathic phospholipid monolayer (Fujimoto and Parton, 2011; Tauchi-Sato et al., 2002) which reduces surface tension at the oil-water (cytosol) interface (Thiam et al., 2013b). This unique surface topology is recognised by a host of proteins involved in LD formation and fate (Ben M'barek et al., 2017; Guo et al., 2008; Kory et al., 2016; Pol et al., 2014; Thiam and Beller, 2017; Thul et al., 2017). Amongst these proteins, those directly associated with the droplet surface typically use amphiphatic helices (AHs), lipid anchors, or monotopic hairpins to do so (Bersuker and Olzmann, 2017; Kory et al., 2016).

The most abundant LD coat protein in mammalian cells is the perilipin (Plin) family of five proteins, Plin1-5. All Plins share a series of 11-mer repeats (11mr) towards the amino terminal which are involved in LD targeting through their ability to form AHs (Bulankina et al., 2009; Copic et al., 2018; McManaman et al., 2003; Nakamura and Fujimoto, 2003; Orlicky et al., 2008; Rowe et al., 2016; Targett-Adams et al., 2003). Plins1-3 and 5 share similar 11mr motifs of about 100 amino acids, whereas Plin4 is distinguished by more numerous copies of the 11mrs, up to 1200 amino acids in length (Copic et al., 2018). Towards their carboxyl terminus, all Plins are predicted to have a 4-helix bundle (4HB) domain (Chong et al., 2011), based on the homology of this region in Plins 1,2,4,5 to that of Plin3, for which the crystal structure was resolved many years ago (Hickenbottom et al., 2004). In Plin3, the 4HB is zipped together by four short β-sheets (Hickenbottom et al., 2004).

Helix bundles conceal hydrophobic residues of helices from the aqueous environment, but the bundle can open up, thereby deploying amphipathic helical structures which can then associate with lipid membranes (Narayanaswami et al., 2010). This behavior suggests that the 4HB of Plins could also be involved in LD binding and some experimental support for the involvement of these regions of perilipins exists (Chong et al., 2011; Garcia et al., 2003; McManaman et al., 2003; Rowe et al., 2016; Subramanian et al., 2004).

What then do perilipins do once associated with LDs? They probably all have a role in reducing surface tension and stabilising LDs, but they are also key regulators of lipid fluxes into and out of LDs. By decorating the surface of LDs, they are ideally placed to regulate the access of hydrolytic lipases, such as adipose tissue triglyceride lipase (ATGL) and hormone sensitive lipase (HSL) to their lipid substrates in the core or possibly on the surface of LDs and several elegant studies have elucidated the mechanisms by which perilipins regulate ATGL and HSL (Brasaemle and Wolins, 2012; Granneman et al., 2007; Itabe et al., 2017; Kimmel et al., 2010; Kimmel and Sztalryd, 2016; Wang et al., 2011; Wang et al., 2009a; Zechner et al., 2012). Studies have also now suggested that exactly how perilipins regulate these lipases differs (Granneman et al., 2009; Patel et al., 2014; Wang et al., 2011). This has important physiological implications as where multiple Plins are present in cells, they bind in a hierarchical manner (Beller et al., 2010; Straub et al., 2008; Wolins et al., 2006). For example, in white adipocytes, Plin1 is ultimately the only Plin at the LD surface, while other Plins are expressed and associate with the LD surface at earlier stages of droplet formation (Brasaemle and Wolins, 2012; Skinner et al., 2009 Wolins et al., 2006). This is important physiologically as evidenced by the phenotype of Plin1 null mice in which basal lipolysis is increased and stimulated lipolysis relatively blunted (Martinez-Botas et al., 2000; Tansey et al., 2001). In humans with loss-of-function Plin1 mutations, Plin2 is up-regulated in white adipose tissue (Kozusko et al., 2015) but it fails to alleviate the severe metabolic consequences of impaired Plin1 function (Gandotra et al., 2011; Kozusko et al., 2015). Plin2 and 3 are widely expressed and mouse knockout studies suggest that Plin2 is particularly important in hepatocytes which do not normally express Plin1 (Libby et al., 2016). Plin3 is reported to localize to droplets emerging from the endoplasmic reticulum (Pol et al., 2014; Skinner et al., 2009) and a recent report suggests that Plin3 null mice manifest increased beiging of white adipocytes (Lee et al., 2018).

Given the physiological importance of the hierarchical binding of perilipins1-3 to LDs, we sought to understand the molecular basis of this phenomenon. Consistent with works from several groups (Bulankina et al., 2009; McManaman et al., 2003; Nakamura and Fujimoto, 2003; Orlicky et al., 2008; Rowe et al., 2016; Targett-Adams et al., 2003), we found that the amino-terminal 11-mer AH repeat regions of Plins1-3 are sufficient for LD localisation. However, importantly, we found that this binding is

highly reversible for all three Plins. In contrast, the binding of the C-terminal 4HB-containing regions varies more substantially and either stabilises or seems to destabilise net binding of the full length proteins. Thus we propose a cooperative binding mechanism which accounts for the observed hierarchical binding properties of this primordial family of LD coat proteins and which is critical for optimal in vivo co-ordination of lipid storage and release.

Results

Comparative localisation of Plins1-3 in mammalian cell lines

To directly compare the localisation of Plins1-3, we studied the localization of amino-terminal fluorescently (GFP or mCherry) tagged full-length (FL) Plins, as well as complementary fragments of the proteins containing their predicted '11-mer repeat' (11mr) and '4-helix bundle' (4HB) domains, respectively denoted Plin-N and Plin-C (Figure 1A). The Plin-N and Plin-C boundaries were designed based on the known structure of the 4HB of Plin3 (Hickenbottom et al., 2004) and our own prior characterisation of the 11mr regions of Plins 1-3 (Rowe et al., 2016). In the case of the Plin-N, each of these constructs also included the putative PAT domain, and in the case of the Plin-C domains, each included the full carboxy terminus of the proteins as well. Binding of these domains was primarily studied in oleate loaded human hepatoma derived (Huh7) and HeLa cells in which only Plin2,3 were endogenously expressed, Plin1 being mainly expressed in adipocytes (Figure S1A).

All proteins localized to the LD surface to at least some extent, except for the Plin3-C which was only observed in the cytosol (Figure 1B and S1B). Whereas FL Plin1 was almost entirely localised around LDs and on the endoplasmic reticulum (ER) membranes (Figure S1D,F), FL Plin2 also displayed some cytosolic localization and FL Plin3 was predominantly cytosolic (Figure 1B). Regarding the fragments, in addition to targeting LDs they were all soluble, to some extent, in the cytosol and in the nucleus, especially the Plin3-N (Figure S1C); the only exception being the Plin1-C which was either observed on LDs or ER membrane (Figure S1B,E), like FL Plin1. In contrast, the Plin2-C colocalized with LDs in a minority of cells but was otherwise predominantly cytosolic (Figure S1B,C). These data are summarized in Figure 1C.

In order to validate these data in a different cell line, all of the GFP-tagged constructs were also expressed in a second mammalian cell line (HeLa) where similar localisation patterns were observed (Figure S1G).

Differential binding stability of Plins1-3 on lipid droplets

To assess the stability of Plins and fragments thereof on the surface of LDs, we performed FRAP analyses, by bleaching the fluorescent signal in a voxel incorporating

a cluster of LDs and then recording its recovery (Figure 1B). From the observed recovery rates, we distinguished three patterns (Figure 1D, E): i) proteins that recovered rapidly included FL Plin3 and the Plins2-N,3-N; ii) FL Plin2 and Plin1-N had intermediate recovery times; iii) the Plins1-C,2-C, and particularly FL Plin1 had the slowest recovery rates. The data suggest that FL Plin1 is considerably more stably associated with the LD surface than FL Plin2, which is in turn more stably associated than FL Plin3. The data are consistent with overall affinity reflecting the combined binding stability of the Plin1-3 fragments. For instance, for Plin2 and Plin3, whose N-terminal manifest similar recovery rates (Figure 1D, E), the C-terminal containing the 4HB ultimately determines the differential LD binding affinity between the FL proteins. In fact, FL Plin3 behaved very similarly to the Plin3-N alone, in keeping with the suggestion that the Plin3-C does not associate with the droplet surface.

We recorded slower recovery rates for Plin1-C,2-C than their corresponding N-terminal containing the 11mrs, which suggests that they both stably bind LDs and might have slow 'on' and/or 'off' rates. However, these 4HBs-containing domains manifested different net behaviours: Plin2-C was predominantly cytosolic and only bound to LDs in a minority of cells, whereas Plin1-C mostly bound to LDs and ER membrane (Figure 1C, Figure S1B-F). We hypothesize that the 4HB of Plin3 is stabilised or 'zipped together' by the beta-sheets in the associated ab domain and thus remains largely in the closed conformation seen in its crystal structure (Hickenbottom et al., 2004) (Figure S2A). The beta-sheets are also predicted to be present in Plin2, whereas they are not present in Plin1 (Figure S2B). Consequently, we speculate that the 4HB of Plin1 might have a greater propensity to unfold and hence hence afford Plin1-C a higher membrane/LD 'on' rate than that of Plin2-C, but both could have low 'off' rates.

The high LD and membrane affinity of the Plin1-C was striking. To confirm this result, we co-expressed the Plin1-C with the Plin1-N (Figure 1F), or FL Plin1 (Figure S2C), or FL Plin2 (Figure S2D), and performed dual FRAP analyses. These data confirmed that the Plin1-C associated with LDs more stably than all the other peptides/proteins besides FL Plin1 (Figure 1G).

Evidence indicating that perilipins1-3 compete for LD surface occupancy in vivo

The FRAP analyses provide trends of the relative LD binding affinities of the various peptides studied (Figure 1D,E). However, a limitation of this analysis is that the sources of the signal recovery are not necessarily identical for all conditions. Signal recovery could occur by protein exchange between LDs, or directly from the cytosol, or possibly by lateral diffusion from the ER to LDs. Aditionnally, we lack precise control over the protein expression levels in individual cells (Goedhart et al., 2011). Nevertheless, we took advantage of the variability of cellular expression levels of the proteins to document their competitive binding in co-expression experiments (Kory et al., 2015). In these experiments, cells were transfected with the different plasmids and they expressed the proteins at different levels. We then took cells with variable amounts of each expressed protein and analysed them.

Initially, we co-expressed FL mCherry-Plin1, as a reference protein, with GFP-tagged versions of FL Plin2 (Figure 2A), FL Plin3, the Plin1-N or the Plin1-C region (Figure 2B-D). We quantified the loss of the GFP-tagged fragments as a fraction of the total fluorescence present on the LD surface and used the resulting profile to estimate a critical concentration of the FL Plin1 on LDs required to displace half of the competing protein (see Figure 2A-D graphs). Plin1 completely displaced all other proteins from LDs at high expression levels, to a greater extent than any other FL Plins or fragments thereof. Switching the GFP and mCherry tags on FL Plin 1 and 2 led to very similar results (Figure S2E); endogenous Plin2,3 levels were not affected by such manipulations (Figure S2F) and may behave as GFP-Plin2,3. All competing proteins were displaced into the cytosol except for the Plin1-C, which relocated to the ER membrane (Figure 2D). These experiments corroborate the previous data, insofar as they suggest that Plin1 competes off the other peptides with a range of displacement efficiencies which are similarly ordered (Figure 2E, F) to the single FRAP analysis studies (Figure 1). These findings were also in agreement with dual FRAP analyses in cells co-expressing FL Plin1 and FL Plin2 (Figure S3A) or the Plin1 fragments (Figure S3B-D).

We also observed intermediate situations where Plin1 and Plin2 were enriched on different LDs, suggesting that Plin2 displacement by Plin1 might occur gradually on different LDs (Figure S3E). We next assessed the binding affinity between FL Plin2

and FL Plin3 (Figure S3F). As predicted, Plin2 fully displaced Plin3. FL Plin3 was also displaced by Plin1-N to a similar level to that of FL Plin2; it was even more efficiently displaced by Plin1-C (Figure S3F,G), confirming the highest LD binding affinity of this 4HB-containing domain after FL Plin1 (Figure 2F). We then probed whether the individual domains of Plin1 were sufficient to fully displace FL Plin2 but the data suggest that these domains cannot do so. Instead, we found that FL Plin2 was either on the same LDs as the fragments or there were distinct LDs enriched with either FL Plin2 or the Plin1 fragments (Figure 2G). Such separation was not seen between Plin1-3 fragments (Figure S3H), suggesting that the N-11mr- and the C-4HB-containing domain jointly regulate Plin binding to LD subsets.

The FRAP analysis of the individually expressed Plin1-C,2-C fragments (summarised in Figure 1D) suggests similar recovery rates whereas their steady state localisation is very different (Figure 1B, Figure S1C,E). To explore this in more detail, we used mCherry-Plin1-N as the reference protein and co-expressed it with GFP-tagged versions of the other fragments that localized to LDs (Figure S3H). Higher expression of the Plin1-N displaced the other fragments from the LD surface to some extent. Plin1-C tended to remain at the interface and had the highest critical concentration (Figure S3H), whereas the Plin2-C was barely detectable on the LD surface when co-expressed with the Plin1-N (Figure S3H), or even with the Plin3-N or FL Plin3 (Figure S3I); for this Plin2-4HB-containing domain, crowding the LD surface with proteins seems to be sufficient to fully prevent binding to the droplet surface, consistent with our previous suggestion that the 4HB-containing domain of Plin2 has a much lower LD 'on' rate than that of Plin1. Regarding the 11mr-containing domains of Plins2,3, they were more readily displaced than the Plin1-C, and at very similar levels (Figure 2H).

In summary, the kinetic (FRAP data in Figure 1) and steady state (Figure 2) data suggest that the 11mr-containing domains of Plin1,2 have similar binding affinities, both apparently higher than that of Plin3. The 4HB-containing domain of Plin3 does not bind LDs on its own in either of the cell types we studied. The 4HB-containing domain of Plin2 only associates with LDs when LD surface protein coverage allows it to do so, whereas that of Plin1 is almost always associated with membranes.

A truncation mutant of Plin3-C manifests enhanced LD localisation

The 4HB structure of Plin3 is 'zipped' together by short β-sheets (Figure S2A, (Hickenbottom et al., 2004)). In order to test the hypothesis that this prevents unfolding and subsequent membrane association of the helix bundle, we generated a truncated version of Plin3 (Plin3 1-413, referred to herein as Plin3-β) lacking the β-sheets, which follow the sequences for the helices constituting the 4HB and 'zip' the helix bundle together. When expressed in oleate loaded Huh7 cells, GFP-Plin3-β consistently localized around LDs to a greater extent than GFP-Plin3 whose signal was often very faint around the LDs (Figure S2H). When co-expressed with mCherry-Plin3, GFP-Plin3-β almost entirely displaced mCherry-Plin3 from LDs (Figure 2I, S2I), strongly suggesting that the Plin3-β mutation enhances LD surface association. This observation is not a result of the GFP/mCherry tags themselves, as GFP-Plin3 largely just colocalized with co-expressed mCherry-Plin3 (Figure 2I). This result is consistent with the suggestion that the β-sheets in the 4HB of Plin3 influence unfolding and hence the propensity to associate with hydrophobic membranes. However, in individual FRAP experiments, Plin3-β recovery was rapid and similar to that of FL Plin3 (Figure 2J-L). We deduce that the Plin3-β mutation only marginally increases LD binding affinity and that this difference is below the resolution of the FRAP analysis in this setting.

In vitro analysis of the binding mode of Plins on an oil-water interface

Theoretically a protein with both membrane binding and soluble domains has the same membrane lateral diffusivity as the binding domain alone, because of the higher viscosity of the membrane than the aqueous phase (supplementary text) (Figure 3A), but the soluble domain of the protein might enhance membrane 'fall off' of the protein into the aqueous phase (Figure 3A). If, however, the soluble domain also interacts with the membrane, the diffusivity of the protein will be reduced, and this additional membrane binding domain is also predicted to reduce the protein membrane 'fall off' (Figure 3A). We hypothesize that the 11mr-containing domains of Plin1-3, Plin1-3-N, constitute the primary LD localisation motif and that this LD association is consistently stabilised by the 4HB-containing domain in Plin1, under optimal conditions in Plin2, but not in Plin3; at least in the conditions we have tested.

In order to test this hypothesis, the GFP or mCherry tagged Plin1-N or FL Plins1-3 were individually expressed in cells, and LDs bound by these proteins were next

purified. This isolated LD fraction was then encapsulated in buffer-in-triolein artificial emulsion droplets and mixed (Figure 3B); this manipulation resulted in the transfer of the proteins to the buffer-in-oil inverted droplet surface as described previously (Kory et al., 2015) (Figure 3B). FRAP analysis was then used to probe the lateral mobility of GFP and mCherry tagged proteins (Figure 3C), and droplet binding stability was evaluated by comparing the tendency of the proteins to transfer off the buffer-oil interface into the buffer lumen in shrinking droplets (due to evaporation of water) (Figure 3D).

FL mCherry-Plin1 recovered more slowly than the GFP-Plin1-N confirming that the Plin1-C contributes to the binding (Figure 3E). This result was supported by comparing the surface-bound fraction in shrinking buffer-in-oil droplets with both peptides at their surface (surface/lumen signal in Figure 3F): FL Plin1 remained at the interface whilst the surface concentration of Plin1-N decreased. These two sets of experiments were repeated with the same peptides but with switched tags in order to show that the GFP and mCherry tags did not influence the data (Figure S4A-B, S4C-D). FL Plin2 also diffused more slowly than Plin1-N, suggesting that its 4HB is also involved in binding to the artificial oil-water interface (Figure 3G). In this experiment, we think that the 4HB in Plin2 does unfold and localise at this 'naked' interface, which is optimal for the binding of Plin2-C. However, during surface shrinkage (Figure 3H), Plin2 'fell off' the interface at a similar level to the Plin1-N (Figure 3H). This data suggests that surface shrinkage increased protein crowding, which favoured re-folding of the 4HB in Plin2-C and solubilisation of the FL Plin2 within the aqueous droplet lumen.

FL Plin3 behaved similarly to the Plin1-N, supporting our previous observations that its 4HB is not involved in LD binding (Figures 3I,J). Finally, we also used Plin1-C as the reference protein and compared it to FL Plin1 and FL Plin2 (Figure S4C-F). The data were similar to what we had seen with the Plin1-N, e.g. FL Plin1,2 diffuses more slowly on the initially naked oil-water interface than the single 4HB domain, but droplet shrinkage causes similar fall off rates for this domain and FL Plin2.

Collectively, these data affirm the suggestion that the 11mrs in Plin-N sense the droplet surface and that the 4HBs in Plin-C regulate the relative binding affinity and stability

of Plin1-3 on LDs, thus accounting, at least in part, for the observed net 'hierarchical' binding of Plin1-3.

The 11-mer repeat of Plin1 associates reversibly with an artificial oil-water interface

The involvement of the 11mr regions in LD localisation of all known Plins is increasingly well established, by several independent groups including our own (Bulankina et al., 2009; Copic et al., 2018; McManaman et al., 2003; Nakamura and Fujimoto, 2003; Orlicky et al., 2008; Rowe et al., 2016; Targett-Adams et al., 2003). We also showed that these regions could mediate targeting of human perilipins1-3 to LDs in Saccharomyces cerevisiae strongly suggesting that this process did not require interaction with additional proteins. Copic et al. have very recently reported similar findings using 11mr regions of Plin4 (Copic et al., 2018). They also showed that purified fragments of the Plin4 11mr regions could associate with LDs in vitro. We previously purified a fragment of Plin1 from amino acids 93 to 192, which includes its predicted 11mr region (Figure 1A), and showed that this domain is unstructured in solution but folds into α-helices in the presence of detergent micelles (Rowe et al., 2016). Its behaviour was compared with that of a mutant in which one neutral leucine residue was substituted with a negatively-charged aspartate residue (L143D) on the hydrophobic face of the predicted AH.

Lipoprotein particles are physically similar to lipid droplets in terms of having a central neutral lipid core surrounded by a phospholipid monolayer. In this case, apolipoproteins associate with the lipoprotein surface (and its core in some instances) where they regulate lipases in a high analogous manner to the perilipins. How they interact with the droplet interface has been extensively characterised using oil droplet tensiometry (Meyers et al., 2012; Mitsche and Small, 2011; Rathnayake et al., 2014; Small et al., 2009). Given these similarities we sought to document the behaviour of the wildtype (WT) and L143D mutant 11mr region of Plin1 in this experimental paradigm (Figure 4A). Initially, a naked triolein-in-water droplet was generated, with an interfacial tension of around ~ 32 mN/m – this value translates an energy cost per unit surface, thus a tension, of oil in contact with water. Equal amounts of the WT or L143D peptides were then added to the solution and surface tension fell from ~ 32 mN/m to an equilibrium tension of ~ 16.3 mN/m for WT and 18.4 mN/m for L143D, meaning that

the peptides adsorbed to the interface to reach an equilibrium density (Figure 4B) – by absorbing to the interface, the peptides masked the interface, which decreased the tension at the oil-water interface. Varying the peptide concentrations revealed that equilibrium tension was consistently lower for WT than for the L143D mutant peptide (Figure 4C), meaning that, for a given concentration, the WT peptide was always consistently better at masking the oil-water interface and decreasing the surface tension.

To assess the reversibility of peptide association, the droplet surface area was rapidly reduced, to modulate the surface protein density (Figure 4A), and then re-expanded. This perturbation immediately reduced surface tension before it almost returned to the initial equilibrium value (Figure 4D). Re-expansion of the droplet surface area resulted in a rapid increase in surface tension followed by a gradual return to the equilibrium tension. This pattern was largely repeated with further larger compressions and was also similar to the L143D mutant peptide (Figure S5A). We interpret these data as indicating that the initial surface compression results in a fall in surface tension as the protein density at the interface rapidly rises (Figure 4A, middle panel) but this is then relieved by expulsion of some of the peptide from the interface to restore equilibrium (Figure 4A, right panel). Re-expansion increases surface tension but the peptides then re-associate with the interface restoring surface tension back to equilibrium. For comparison, when a similar experiment is done using apolipoprotein B, compression led to a net decrease of tension and no protein desorption occurs, whereas with peptides derived from apolipoprotein C, similar behaviour is observed (Meyers et al., 2015; Meyers et al., 2012; Wang et al., 2009b).

Collectively these data demonstrate reversible binding of the Plin1 11mr to the oil-water interface, as seen *in vivo* (Figure 1B, 1D), highlight the impact of changes in the peptide sequence on the nascent amphipathic helices, and finally confirm that this domain cannot withstand high surface protein densities which induce its desorption.

The 11-mer repeat of Plin1 displaces the L143D mutant

In order to assess the potential for 11mr peptides to 'compete' for surface occupancy, we initially added the L143D mutant peptide and, as before, surface tension fell to ~18.4 mN/m (Figure 4E). Compression of the interface barely changed the equilibrium tension (Figure 4E), as already observed in Figure 4D. WT peptide was then added and

the equilibrium tension fell further to ~ 15.6 mN/m, as if it was alone on the surface (Figure 4B), suggesting that it displaced the L143D mutant from the interface. Indeed, compressing and re-expanding the droplet resulted in a different surface tension restoring profile (Figure 4E, arrowhead). We interpret this last observation as suggesting that initially both the WT and L143D mutant peptides re-associate with the expanded surface so surface tension falls rapidly towards ~18.4 mN/m but over time the WT entirely displaces the L143D peptide restoring surface tension to ~15.6 mN/m.

Proteins displace the 11-mer repeat from the droplet surface more effectively than phospholipids

To more closely reproduce the in vivo situation, phospholipids (POPC) were added to the triolein-water interface reducing surface tension from ~ 32 to ~ 26 mN/m (Figure S5B). Addition of the WT Plin1 peptide (Figure S5B) prompted a further reduction in surface tension to a new equilibrium of ~13.4 mN/m, which was lower than that observed with the peptide alone (on TO/water interface) (Figure 4B). Here too, the L143D Plin1 mutant peptide (Figure S5B) reduced surface tension less effectively to ~ 16.5 mN/m. Interestingly, when compressed and re-expanded, the surface tension profiles were slightly different than what was observed in the absence of POPC: following compression and the initial fall in surface tension, surface tension rose but remained at a new equilibrium below the baseline equilibrium (compare equilibrium tension after compression in Figure 4D and Figure 4F, and Figure S5A and S5B). We interpret these data as indicating that the peptide is only partially removed from the interface upon surface compression and can then rapidly 'snap' back onto the interface when it is re-expanded. This phenomenon was more striking with the WT than with the mutant peptide (Figure S5B) and was also apparent in competition experiments undertaken after addition of phospholipids to the TO/W interface (Figure S5C).

We next repeated the compression experiments with a range of concentrations of the WT and mutant peptides enabling us to estimate the maximum lateral surface pressure exerted by compression that the peptides can withstand without being ejected (Figure 4G); we called this pressure Π_{max}. We found that Π_{max} of the WT and mutant (Figure 4G, Figure S5D) was consistently higher in the presence of POPC. This result suggests that phospholipids aid retention of the peptides on the interface at least in this context.

As anticipated, the exclusion pressure for L143D was lower than that for WT peptide before and after the addition of POPC (Figure 4H, Figure S5D).

Discussion

Lipid storage is carefully regulated in order to both alleviate potential lipotoxicity and to provide a rapidly available energy source when needed in either a cell autonomous manner or, in metazoans, by other more highly oxidative tissues. In vertebrates, white adipocytes constitute the primary lipid storage cell type for the whole organism, whereas other more oxidative tissues like the liver and skeletal muscle have progressively lower tendencies to accumulate lipids. In each of these different tissue/cell types, cellular lipid fluxes are finely coordinated in keeping with their respective physiological functions. Lipid flux is regulated at multiple levels both outside i.e. blood flow and intravascular lipolysis, and within individual cell types i.e. intracellular lipolysis. Perilipins play key roles in regulating intracellular lipid storage and lipolysis, and are significant contributors in determining the fate of lipids in cells. A key aspect of how they contribute to these tissue specific differences in lipid flux is through differential tissue distribution i.e. they are expressed at different levels in different tissues. Then, where more than one member of the Plin family is expressed in a particular cell type, they bind to LDs in a differential manner (Beller et al., 2010; Hsieh et al., 2012; Straub et al., 2008; Wolins et al., 2006). Importantly, binding to the LD surface is also a major determinant of overall expression levels of Plin1,2, as both are subject to proteosomal degradation when not bound to LDs, whereas Plin3 is stable in the cytoplasm (Masuda et al., 2006; Xu et al., 2006; Xu et al., 2005). This post-transcriptional regulation of Plin expression may contribute to the specificity of LD association, which is another important feature of perilipin biology.

Our data addresses two main questions: firstly, how do Plins1-3 recognise and localise on LDs, and, what determines their apparently hierarchical and competitive binding to LDs? In keeping with our own prior work in yeast suggesting that the 11mr regions of human Plins1-3 was sufficient to mediate LD localisation in this ancient cell type (Rowe et al., 2016) and in which the 11mrs were unlikely to interact with other host proteins given the evolutionary distance between humans and Saccharomyces cerevisiae, the data suggest that the 11mr acts as a general and primary LD sensing motif. These data are also consistent with several other reports (Bulankina et al., 2009; McManaman et al., 2003; Nakamura and Fujimoto, 2003; Orlicky et al., 2008; Rowe et al., 2016; Targett-Adams et al., 2003) and with data suggesting that other 11mr domain containing proteins such as α-synuclein can also localise to LDs (Brasaemle,

2007; Cole et al., 2002; Thiam et al., 2013a). We envisage the 11mr regions behaving as nascent helices which only fold into an AH in the presence of 'surface voids' on the LDs. Importantly, at least under the conditions we have tested, the binding affinities of the 11mr regions seem similar amongst Plin1-3 (Figure 1D,E and Figure 2H). However, in vitro experiments with the point mutant L143D which associates less effectively with an artificial droplet interface than the WT peptide indicate that differences in the amino acid sequences of the nascent amphipathic helices can result in peptides 'forcing' other peptides with lower membrane affinity off the interface. There may well be subtle differences in the binding affinity of this region amongst Plin1-3 related to the differences in the compositions of their amphipathic helices. For example, it has been recently proposed that tryptophan or phenylalanine are important residues for LD binding selectivity (Prevost et al., 2018). Two of these residues are present in the Plin1 11mr but there are none in either the Plin2 or Plin3 11mr regions. However the Plin2,3 11-mers localise effectively to LDs (Figure 1), meaning that although these bulky hydrophobic residues might aid LD binding selectivity they are not essential; this conclusion is supported by the LD binding of the Plin4 11mrs which also lack these amino acids (Copic et al., 2018).

The association of the 11mr regions with LDs is significantly enhanced by the presence of an additional membrane binding domain, which encompasses the 4HB region, as illustrated by both in vivo and in vitro experiments. These findings are consistent with prior reports suggesting that this region of Plin1 was involved in LD targeting (Garcia et al., 2003) and help to reconcile these data with data highlighting the importance of the 11mr regions. However, whereas the 4HB region of Plin1 is consistently associated with LDs, and when not on LDs, it associates with the ER (Figure 1C, Figure S1E,F), that of Plin2 is less consistently associated with LDs and is readily displaced by protein crowding induced by co-expression of other proteins or peptides which localise to LDs (Figure S3H, S3I). In our studies, the Plin3 4HB-containing region (Plin3-C) did not localise to LDs in HuH7 or HeLa cells, in keeping with our prior work in Saccharomyces cerevisiae (Rowe et al., 2016). The 4HB of Plin4 was also recently shown not to localize to LDs (Copic et al., 2018). The behaviors of these 4HBs is generally consistent with their known or predicted ~~(Hickenbottom et al., 2004)~~ structures (Hickenbottom et al., 2004). Indeed, except for Plin1, the 4HB is zipped together by four-stranded β-sheets in a smaller αβ domain (Hickenbottom et al., 2004)

(Figure S2A,B). Plin1 has one extra exon at its C-terminus (404-522) in vertebrate evolution and the homology to other Plins consequently stops sharp at position 403 (Figure S2B) (Patel et al., 2014). The β-sheet is hence most likely absent in the Plin1 structure and the 4HB is therefore probably not stabilized as in other Plins (Figure S2A), thereby potentially explaining its instability in solution and greater propensity to open up and associate with phospholipid membranes. Our data suggest that the Plin2 4HB is likely to open up in cells, though exactly how this is regulated is not yet clear to us. We also cannot formally exclude the possibility that the 4HB of Plin3 can open up in specific circumstances.

In vivo, most cell types with small droplets do not express Plin1, so Plin2 or Plin3 can occupy the LD surface. In cells without or with very few LDs, Plin3 will remain in the cytoplasm ready to associate with new LDs emerging from the ER (Pol et al., 2014), whereas Plin2 expression will be very low and will depend on the presence of LDs. Plin1 expression is regulated by PPARγ and it is for example only expressed at a relatively late stage of adipocyte differentiation (Arimura et al., 2004), when cells possess fairly large LDs to which it can bind. In adipocytes with smaller LDs, we suspect that Plin2 displaces Plin3 from the surface of LDs by virtue of the greater tendency of its 4HB to unfold and associate with the LD surface. Later on, when Plin1 is expressed it duly replaces Plin2 from the LD surface. This is particularly important physiologically as evidenced by the increase in basal lipolysis observed in Plin1 null mice, in which Plin2 replaces Plin1 on LDs (Tansey et al., 2001). In humans, loss-of-function Plin1 mutations also alter lipolytic regulation and result in severe metabolic disease despite compensatory up-regulation of Plin2 (Kozusko et al., 2015; Tansey et al., 2003).

In summary, our data suggests that the nascent amphipathic helices encoded by the 11 mer repeat regions, present in all Plins, constitute the initial LD sensing domain. The subsequent stability of Plins1-3 on LDs is then heavily influenced by the differential propensities of their 4HB domains to unfold and bind to the LD surface. Ultimately we suggest that the combined affinities of these two domains underpins the hierarchical LD binding which we and others have observed, and which is essential for optimal fatty acid traffic into and out of cellular LDs.

AUTHOR CONTRIBUTIONS

DMS, DBS, and ART conceived and designed experiments with help from VS. MLM, RGK purified and validated the Plin1 11mer repeat peptide and DMS performed the oil-drop tensiometry studies with help from CE and HH. LD and SP cloned the Plin fragments for cellular imaging and in vitro studies which were carried out by DA, KBM and ART. DS and ART wrote the manuscript and all the authors reviewed and edited it.

ACKNOWLEDGEMENTS

The authors thank Drs. W. Urbach, F. Pincet for helpful discussions. D.B.S. is supported by the Wellcome Trust (WT 107064), the MRC Metabolic Disease Unit, the National Institute for Health Research (NIHR) Cambridge Biomedical Research Centre and NIHR Rare Disease Translational Research Collaboration. A.R.T is supported by the ANR-MOBIL, ANRS, Programme Emergence de la Ville de Paris, PSL, and ATIP-Avenir, and D.A. is supported by ANRS.

References

Arimura, N., Horiba, T., Imagawa, M., Shimizu, M., and Sato, R. (2004). The peroxisome proliferator-activated receptor gamma regulates expression of the perilipin gene in adipocytes. The Journal of biological chemistry *279*, 10070-10076.

Beller, M., Bulankina, A.V., Hsiao, H.H., Urlaub, H., Jackle, H., and Kuhnlein, R.P. (2010). PERILIPIN-dependent control of lipid droplet structure and fat storage in Drosophila. Cell metabolism *12*, 521-532.

Ben M'barek, K., Ajjaji, D., Chorlay, A., Vanni, S., Foret, L., and Thiam, A.R. (2017). ER Membrane Phospholipids and Surface Tension Control Cellular Lipid Droplet Formation. Developmental cell *41*, 591-604 e597.

Bersuker, K., and Olzmann, J.A. (2017). Establishing the lipid droplet proteome: Mechanisms of lipid droplet protein targeting and degradation. Biochimica et biophysica acta *1862*, 1166-1177.

Brasaemle, D.L. (2007). Thematic review series: adipocyte biology. The perilipin family of structural lipid droplet proteins: stabilization of lipid droplets and control of lipolysis. Journal of lipid research *48*, 2547-2559.

Brasaemle, D.L., and Wolins, N.E. (2012). Packaging of fat: an evolving model of lipid droplet assembly and expansion. The Journal of biological chemistry *287*, 2273-2279.

Bulankina, A.V., Deggerich, A., Wenzel, D., Mutenda, K., Wittmann, J.G., Rudolph, M.G., Burger, K.N., and Honing, S. (2009). TIP47 functions in the biogenesis of lipid droplets. The Journal of cell biology *185*, 641-655.

Chong, B.M., Russell, T.D., Schaack, J., Orlicky, D.J., Reigan, P., Ladinsky, M., and McManaman, J.L. (2011). The adipophilin C terminus is a self-folding membrane-binding domain that is important for milk lipid secretion. Journal of Biological Chemistry *286*, 23254-23265.

Cole, N.B., Murphy, D.D., Grider, T., Rueter, S., Brasaemle, D., and Nussbaum, R.L. (2002). Lipid droplet binding and oligomerization properties of the Parkinson's disease protein alpha-synuclein. The Journal of biological chemistry *277*, 6344-6352.

Copic, A., Antoine-Bally, S., Gimenez-Andres, M., Garay, C.L.T., Antonny, B., Manni, M.M., Pagnotta, S., GUIHOT, J., and Jackson, C.L. (2018). A giant amphipathic helix from a perilipin that is adapted for coating lipid droplets. bioRxiv, 276238.

Fujimoto, T., and Parton, R.G. (2011). Not just fat: the structure and function of the lipid droplet. Cold Spring Harbor perspectives in biology *3*.

Gandotra, S., Le Dour, C., Bottomley, W., Cervera, P., Giral, P., Reznik, Y., Charpentier, G., Auclair, M., Delepine, M., Barroso, I.*, et al.* (2011). Perilipin deficiency and autosomal dominant partial lipodystrophy. The New England journal of medicine *364*, 740-748.

Gao, Q., Binns, D.D., Kinch, L.N., Grishin, N.V., Ortiz, N., Chen, X., and Goodman, J.M. (2017). Pet10p is a yeast perilipin that stabilizes lipid droplets and promotes their assembly. The Journal of cell biology *216*, 3199-3217.

Garcia, A., Sekowski, A., Subramanian, V., and Brasaemle, D.L. (2003). The central domain is required to target and anchor perilipin A to lipid droplets. The Journal of biological chemistry *278*, 625-635.

Goedhart, J., van Weeren, L., Adjobo-Hermans, M.J., Elzenaar, I., Hink, M.A., and Gadella, T.W., Jr. (2011). Quantitative co-expression of proteins at the single cell level--application to a multimeric FRET sensor. PloS one *6*, e27321.

Granneman, J.G., Moore, H.P., Granneman, R.L., Greenberg, A.S., Obin, M.S., and Zhu, Z. (2007). Analysis of lipolytic protein trafficking and interactions in adipocytes. The Journal of biological chemistry *282*, 5726-5735.
Granneman, J.G., Moore, H.P., Krishnamoorthy, R., and Rathod, M. (2009). Perilipin controls lipolysis by regulating the interactions of AB-hydrolase containing 5 (Abhd5) and adipose triglyceride lipase (Atgl). The Journal of biological chemistry *284*, 34538-34544.
Greenberg, A.S., Egan, J.J., Wek, S.A., Garty, N.B., Blanchette-Mackie, E.J., and Londos, C. (1991). Perilipin, a major hormonally regulated adipocyte-specific phosphoprotein associated with the periphery of lipid storage droplets. The Journal of biological chemistry *266*, 11341-11346.
Guo, Y., Walther, T.C., Rao, M., Stuurman, N., Goshima, G., Terayama, K., Wong, J.S., Vale, R.D., Walter, P., and Farese, R.V. (2008). Functional genomic screen reveals genes involved in lipid-droplet formation and utilization. Nature *453*, 657-661.
Hickenbottom, S.J., Kimmel, A.R., Londos, C., and Hurley, J.H. (2004). Structure of a lipid droplet protein; the PAT family member TIP47. Structure *12*, 1199-1207.
Hsieh, K., Lee, Y.K., Londos, C., Raaka, B.M., Dalen, K.T., and Kimmel, A.R. (2012). Perilipin family members preferentially sequester to either triacylglycerol-specific or cholesteryl-ester-specific intracellular lipid storage droplets. Journal of cell science *125*, 4067-4076.
Itabe, H., Yamaguchi, T., Nimura, S., and Sasabe, N. (2017). Perilipins: a diversity of intracellular lipid droplet proteins. Lipids in health and disease *16*, 83.
Kimmel, A.R., Brasaemle, D.L., McAndrews-Hill, M., Sztalryd, C., and Londos, C. (2010). Adoption of PERILIPIN as a unifying nomenclature for the mammalian PAT-family of intracellular lipid storage droplet proteins. Journal of lipid research *51*, 468-471.
Kimmel, A.R., and Sztalryd, C. (2016). The Perilipins: Major Cytosolic Lipid Droplet-Associated Proteins and Their Roles in Cellular Lipid Storage, Mobilization, and Systemic Homeostasis. Annual review of nutrition *36*, 471-509.
Kory, N., Farese, R.V., Jr., and Walther, T.C. (2016). Targeting Fat: Mechanisms of Protein Localization to Lipid Droplets. Trends in cell biology *26*, 535-546.
Kory, N., Thiam, A.R., Farese, R.V., Jr., and Walther, T.C. (2015). Protein Crowding Is a Determinant of Lipid Droplet Protein Composition. Developmental cell *34*, 351-363.
Kozusko, K., Tsang, V., Bottomley, W., Cho, Y.H., Gandotra, S., Mimmack, M.L., Lim, K., Isaac, I., Patel, S., Saudek, V., *et al.* (2015). Clinical and molecular characterization of a novel PLIN1 frameshift mutation identified in patients with familial partial lipodystrophy. Diabetes *64*, 299-310.
Lee, Y.K., Sohn, J.H., Han, J.S., Park, Y.J., Jeon, Y.G., Ji, Y., Dalen, K.T., Sztalryd, C., Kimmel, A.R., and Kim, J.B. (2018). Perilipin 3 Deficiency Stimulates Thermogenic Beige Adipocytes Through PPARalpha Activation. Diabetes *67*, 791-804.
Libby, A.E., Bales, E., Orlicky, D.J., and McManaman, J.L. (2016). Perilipin-2 Deletion Impairs Hepatic Lipid Accumulation by Interfering with Sterol Regulatory Element-binding Protein (SREBP) Activation and Altering the Hepatic Lipidome. The Journal of biological chemistry *291*, 24231-24246.
Martinez-Botas, J., Anderson, J.B., Tessier, D., Lapillonne, A., Chang, B.H., Quast, M.J., Gorenstein, D., Chen, K.H., and Chan, L. (2000). Absence of perilipin results in leanness and reverses obesity in Lepr(db/db) mice. Nature genetics *26*, 474-479.

Masuda, Y., Itabe, H., Odaki, M., Hama, K., Fujimoto, Y., Mori, M., Sasabe, N., Aoki, J., Arai, H., and Takano, T. (2006). ADRP/adipophilin is degraded through the proteasome-dependent pathway during regression of lipid-storing cells. Journal of lipid research *47*, 87-98.
McManaman, J.L., Zabaronick, W., Schaack, J., and Orlicky, D.J. (2003). Lipid droplet targeting domains of adipophilin. Journal of lipid research *44*, 668-673.
Meyers, N.L., Larsson, M., Olivecrona, G., and Small, D.M. (2015). A Pressure-dependent Model for the Regulation of Lipoprotein Lipase by Apolipoprotein C-II. The Journal of biological chemistry *290*, 18029-18044.
Meyers, N.L., Wang, L., Gursky, O., and Small, D.M. (2013). Changes in helical content or net charge of apolipoprotein C-I alter its affinity for lipid/water interfaces. Journal of lipid research *54*, 1927-1938.
Meyers, N.L., Wang, L., and Small, D.M. (2012). Apolipoprotein C-I binds more strongly to phospholipid/triolein/water than triolein/water interfaces: a possible model for inhibiting cholesterol ester transfer protein activity and triacylglycerol-rich lipoprotein uptake. Biochemistry *51*, 1238-1248.
Mitsche, M.A., and Small, D.M. (2011). C-terminus of apolipoprotein A-I removes phospholipids from a triolein/phospholipids/water interface, but the N-terminus does not: a possible mechanism for nascent HDL assembly. Biophysical journal *101*, 353-361.
Mitsche, M.A., and Small, D.M. (2013). Surface pressure-dependent conformation change of apolipoprotein-derived amphipathic alpha-helices. Journal of lipid research *54*, 1578-1588.
Mitsche, M.A., Wang, L., and Small, D.M. (2010). Adsorption of egg phosphatidylcholine to an air/water and triolein/water bubble interface: use of the 2-dimensional phase rule to estimate the surface composition of a phospholipid/triolein/water surface as a function of surface pressure. The journal of physical chemistry B *114*, 3276-3284.
Nakamura, N., and Fujimoto, T. (2003). Adipose differentiation-related protein has two independent domains for targeting to lipid droplets. Biochemical and biophysical research communications *306*, 333-338.
Narayanaswami, V., Kiss, R.S., and Weers, P.M. (2010). The helix bundle: a reversible lipid binding motif. Comparative biochemistry and physiology Part A, Molecular & integrative physiology *155*, 123-133.
Orlicky, D.J., Degala, G., Greenwood, C., Bales, E.S., Russell, T.D., and McManaman, J.L. (2008). Multiple functions encoded by the N-terminal PAT domain of adipophilin. Journal of cell science *121*, 2921-2929.
Patel, S., Yang, W., Kozusko, K., Saudek, V., and Savage, D.B. (2014). Perilipins 2 and 3 lack a carboxy-terminal domain present in perilipin 1 involved in sequestering ABHD5 and suppressing basal lipolysis. Proceedings of the National Academy of Sciences *111*, 9163-9168.
Pol, A., Gross, S.P., and Parton, R.G. (2014). Review: biogenesis of the multifunctional lipid droplet: lipids, proteins, and sites. The Journal of cell biology *204*, 635-646.
Prevost, C., Sharp, M.E., Kory, N., Lin, Q., Voth, G.A., Farese, R.V., Jr., and Walther, T.C. (2018). Mechanism and Determinants of Amphipathic Helix-Containing Protein Targeting to Lipid Droplets. Developmental cell *44*, 73-86 e74.
Rathnayake, S.S., Mirheydari, M., Schulte, A., Gillahan, J.E., Gentit, T., Phillips, A.N., Okonkwo, R.K., Burger, K.N., Mann, E.K., Vaknin, D.*, et al.* (2014). Insertion of

apoLp-III into a lipid monolayer is more favorable for saturated, more ordered, acyl-chains. Biochimica et biophysica acta *1838*, 482-492.
Rowe, E.R., Mimmack, M.L., Barbosa, A.D., Haider, A., Isaac, I., Ouberai, M.M., Thiam, A.R., Patel, S., Saudek, V., Siniossoglou, S*., et al.* (2016). Conserved amphipathic helices mediate lipid droplet targeting of perilipins 1-3. The Journal of biological chemistry.
Skinner, J.R., Shew, T.M., Schwartz, D.M., Tzekov, A., Lepus, C.M., Abumrad, N.A., and Wolins, N.E. (2009). Diacylglycerol enrichment of endoplasmic reticulum or lipid droplets recruits perilipin 3/TIP47 during lipid storage and mobilization. The Journal of biological chemistry *284*, 30941-30948.
Small, D.M., Wang, L., and Mitsche, M.A. (2009). The adsorption of biological peptides and proteins at the oil/water interface. A potentially important but largely unexplored field. Journal of lipid research *50 Suppl*, S329-334.
Straub, B.K., Stoeffel, P., Heid, H., Zimbelmann, R., and Schirmacher, P. (2008). Differential pattern of lipid droplet-associated proteins and de novo perilipin expression in hepatocyte steatogenesis. Hepatology *47*, 1936-1946.
Subramanian, V., Garcia, A., Sekowski, A., and Brasaemle, D.L. (2004). Hydrophobic sequences target and anchor perilipin A to lipid droplets. Journal of lipid research *45*, 1983-1991.
Tansey, J.T., Huml, A.M., Vogt, R., Davis, K.E., Jones, J.M., Fraser, K.A., Brasaemle, D.L., Kimmel, A.R., and Londos, C. (2003). Functional studies on native and mutated forms of perilipins. A role in protein kinase A-mediated lipolysis of triacylglycerols. The Journal of biological chemistry *278*, 8401-8406.
Tansey, J.T., Sztalryd, C., Gruia-Gray, J., Roush, D.L., Zee, J.V., Gavrilova, O., Reitman, M.L., Deng, C.X., Li, C., Kimmel, A.R*., et al.* (2001). Perilipin ablation results in a lean mouse with aberrant adipocyte lipolysis, enhanced leptin production, and resistance to diet-induced obesity. Proceedings of the National Academy of Sciences of the United States of America *98*, 6494-6499.
Targett-Adams, P., Chambers, D., Gledhill, S., Hope, R.G., Coy, J.F., Girod, A., and McLauchlan, J. (2003). Live cell analysis and targeting of the lipid droplet-binding adipocyte differentiation-related protein. The Journal of biological chemistry *278*, 15998-16007.
Tauchi-Sato, K., Ozeki, S., Houjou, T., Taguchi, R., and Fujimoto, T. (2002). The surface of lipid droplets is a phospholipid monolayer with a unique Fatty Acid composition. The Journal of biological chemistry *277*, 44507-44512.
Thiam, A.R., Antonny, B., Wang, J., Delacotte, J., Wilfling, F., Walther, T.C., Beck, R., Rothman, J.E., and Pincet, F. (2013a). COPI buds 60-nm lipid droplets from reconstituted water-phospholipid-triacylglyceride interfaces, suggesting a tension clamp function. Proceedings of the National Academy of Sciences of the United States of America *110*, 13244-13249.
Thiam, A.R., and Beller, M. (2017). The why, when and how of lipid droplet diversity. Journal of cell science *130*, 315-324.
Thiam, A.R., Farese, R.V., Jr., and Walther, T.C. (2013b). The biophysics and cell biology of lipid droplets. Nature reviews Molecular cell biology *14*, 775-786.
Thul, P.J., Tschapalda, K., Kolkhof, P., Thiam, A.R., Oberer, M., and Beller, M. (2017). Targeting of the Drosophila protein CG2254/Ldsdh1 to a subset of lipid droplets. Journal of cell science *130*, 3141-3157.
Wang, H., Bell, M., Sreenivasan, U., Hu, H., Liu, J., Dalen, K., Londos, C., Yamaguchi, T., Rizzo, M.A., Coleman, R*., et al.* (2011). Unique regulation of adipose triglyceride

lipase (ATGL) by perilipin 5, a lipid droplet-associated protein. The Journal of biological chemistry *286*, 15707-15715.
Wang, H., Hu, L., Dalen, K., Dorward, H., Marcinkiewicz, A., Russell, D., Gong, D., Londos, C., Yamaguchi, T., Holm, C.*, et al.* (2009a). Activation of hormone-sensitive lipase requires two steps, protein phosphorylation and binding to the PAT-1 domain of lipid droplet coat proteins. The Journal of biological chemistry *284*, 32116-32125.
Wang, L., Martin, D.D., Genter, E., Wang, J., McLeod, R.S., and Small, D.M. (2009b). Surface study of apoB1694-1880, a sequence that can anchor apoB to lipoproteins and make it nonexchangeable. Journal of lipid research *50*, 1340-1352.
Wolins, N.E., Brasaemle, D.L., and Bickel, P.E. (2006). A proposed model of fat packaging by exchangeable lipid droplet proteins. FEBS letters *580*, 5484-5491.
Xu, G., Sztalryd, C., and Londos, C. (2006). Degradation of perilipin is mediated through ubiquitination-proteasome pathway. Biochimica et biophysica acta *1761*, 83-90.
Xu, G., Sztalryd, C., Lu, X., Tansey, J.T., Gan, J., Dorward, H., Kimmel, A.R., and Londos, C. (2005). Post-translational regulation of adipose differentiation-related protein by the ubiquitin/proteasome pathway. The Journal of biological chemistry *280*, 42841-42847.
Zechner, R., Zimmermann, R., Eichmann, T.O., Kohlwein, S.D., Haemmerle, G., Lass, A., and Madeo, F. (2012). FAT SIGNALS--lipases and lipolysis in lipid metabolism and signaling. Cell metabolism *15*, 279-291.

Figure legends

Figure 1

(A) Simplified schematic illustration of the "11-mer repeat" (11mr) and "4-helix bundle" (4HB) domains of Plins1-3 alongside their respective amino acid numbers. PAT domain refers to the conserved amino-terminal region of the protein (black rectangle). Amino acids from 1 to 192, 191 and 204 respectively in Plin1-3 are termed Plin(1-3)-**N**. Amino acids from 193, 192 and 205 to the end of each protein, respectively in Plin1-3, are termed Plin(1-3)-**C**.

(B) FRAP (fluorescence recovery after photobleaching) analysis of full-length (FL) Plins and their complementary fragments containing the predicted 11mr and 4HB domains in a mammalian Huh7 cell line. The protein constructs were fused to GFP on the amino-terminus, except for the Plin2-**N** which had instead a mCherry tag. The left hand panel shows the steady state localization of each protein prior to photobleaching. The insert squares indicate the bleached region in the second panel from the left and then subsequent panels show this region at the indicated times thereafter. Representative image sequence is shown. Each experiment was repeated at least three times. Scale bar, 10 μm.

(C) Relative 'steady state' localisation (LD (lipid droplet)/cytosol/membranes) of tagged Plins1-3 and fragments in Huh7 cells. We considered proteins to be: i) present on LDs when they formed a fluorescent ring around LDs; ii) cytosolic when they were associated with a diffuse fluorescent signal in the cytoplasm; and iii) 'membrane' associated when they were associated with a reticular fluorescent signal in the cytoplasm – in both cases, subsequent analyses showed that this signal colocalised with an endoplasmic reticulum marker. A minimum of 20 cells was analysed for each construct to validate localization of the proteins.

(D) Quantitative analysis of the recovery kinetics of Plins and fragments thereof to the LD surface following FRAP. Data are normalized to both pre- and post-bleach intensities. Curves are exponential fits of the data. Each FRAP experiment was repeated three times and representative recovery rates are shown.

(E) Histogram of characteristic recovery times of the different peptides for experiments in (B, D). The characteristic time 'tau', referred to herein as "recovery time", is obtained by the following exponential fit 1-exp(-t/tau). The value of tau is the average value of all experiments performed in (B, D).

(F) Representative images of a FRAP image sequence of the GFP-tagged Plin1-**C** and mCherry-tagged Plin1-**N** when co-expressed in Huh7 cells. Scale bar, 10 μm. The normalized fluorescence recovery of the bleached LD cluster is shown over time. Curves correspond to exponential fits.

(G) Histogram of the characteristic recovery times of the co-expressed GFP-Plin1-**C** respectively with mCherry-Plin1,2 and the Plin 1-**N**. Black bars correspond to the recovery time of Plin 1-**C** in dual FRAP analysis against FL Plin1, FL Plin2 and the Plin1-**N** that correspond to white bars. This experiment was repeated three times and the value of tau corresponds to the representative images/quantification shown.

Supplementary Figure 1 (related to Figure 1)

(A) Endogenous Plin expression was evaluated by western blot in Huh7, 3T3 D12 adipocytes and Hela cells. Calnexin was used as loading control.

(B) The left hand panel shows the localization (LD (lipid droplet)/cytosol) of the GFP-tagged Plins(1-3)-**C** in Huh7 cells. Scale bar, 10 μm. Zoomed in views of the insets are shown on the right. The fluorescence profiles of lines drawn in the insets are shown on the far right (LD in red, Protein in green). Localization of proteins at the LD surface gives two clear green peaks around the red LD signal. The far right-hand panel shows the % of LDs in cells having the protein at their surface. 15–20 cells were combined for analysis, corresponding to a total number of LDs of ~1500.

(C) Representative images of the relative localization (Nucleus/Cytosol) of GFP-tagged fragments of the Plin(1-3)-**N** (right panel) and Plin(1-3)-**C** (left panel). Scale bar, 10 μm.

(D) Representative image of the GFP-FL Plin1 and mCherry-Sec61 beta colocalization in Huh7 cells. The inset squares indicate colocalization of the two proteins; colocalization was analysed by Fiji, and the Pearson's coefficient reveals a high degree of colocalization (F). Data are expressed as means ± SEM. Scale bar, 10 μm.

(E) Representative image of the Plin1-**C** GFP-tagged and mCherry-Sec61 beta colocalization in Huh7 cells. The inset squares indicate colocalization of the two proteins; colocalization was analysed by Fiji, and the Pearson's coefficient reveals a high degree of colocalization (F). Data are expressed as means ± SEM. Scale bar, 10 μm.

(G) HeLa cells were transfected with GFP-tagged full-length (FL), Plin-**N** and Plin-**C** perilipin constructs. Four hours post transfection, cells were loaded with 400 μM oleic

acid and BODIPY 558/568 C_{12} for 20 h prior to fixing. Cells were imaged using confocal microscopy. Scale bars, 10 μm. Images are representative of 2 – 3 independent experiments.

Supplementary Figure 2 (related to Figure 1 and Figure 2)

A) Carboxy-terminal domain of Plin3 (Hickenbottom et al., 2004) (PDB ID 1szi) consisting of a 4HB (aa 244-412) zipped together by 4 strands of β-sheet (position in the alignment below). Top: topology of the secondary structure elements; bottom left: 3D structure; bottom right: schematic illustration of the 4HB structure with helices represented as cylinders and β-sheets as arrows. The name "4HB" is used for this domain throughout the paper. Homology indicates that the structure of Plins 2, 4 and 5 are very similar in this region while Plin1 does not contain the stabilising β-sheet (Hickenbottom et al., 2004; Rowe et al., 2016).

B) Comparison of the sequences known to form β-sheets in mouse Plin3 (1szi) with corresponding segments in human Plins. The intensity of the blue background indicates the amino acid identity, the bars represent the strands of β-sheet and the arrow depicts the position of the beginning of the Plin1 unique extra exon with evolutionary unrelated sequence.

(C) FRAP analysis of the Plin1-**C** and FL Plin1 co-expressed in Huh7 cells. The inset squares indicate the bleached region in the second panel from the left and then subsequent panels show this region immediately after bleaching and then at the indicated times thereafter. Scale bar, 10 μm. The experiment was repeated twice and the normalized fluorescence intensity evolution of the bleached LD cluster is shown for the displayed representative sequence.

(D) FRAP analysis of the Plin1-**C** and FL Plin2 co-expressed in Huh7 cells. The insert squares indicate the bleached region in the second panel from the left and then subsequent panels show this region immediately after bleaching and then at the indicated times thereafter. Scale bar, 10 μm. The experiment was repeated three times and the normalized fluorescence intensity evolution of the bleached LD cluster is shown for the displayed representative sequence.

(E) GFP-FL Plin1 co-expression and LD colocalization with mCherry-FL Plin2 in Huh7 cells. The insert squares indicate the colocalization region of corresponding proteins to the LD surface. The relative bound fraction level is reported on the right panel and indicates that GFP-FL Plin1 displaces mCherry-FL Plin2 from the LD surface. A similar displacement is observed in Figure 2A but with switched tags. GFP/mCherry does not affect the behaviour of the constructs. Each experimental dot corresponds to an average of the signal on 10 to 20 LDs. Scale bar, 10 µm.

(F) Expression of endogenous Plin2,3 was evaluated by western blot in Huh7 cells transfected with eGFP-Plin1 (left panel) and eGFP-Plin2 (right panel). β-actin was used as loading control.

(G) Western blot analysis using antibodies to endogenous Plin3 in Huh7 cells transfected with eGFP-Plin3 and eGFP- Plin3-β. GAPDH was used as loading control.

(H) Images of eGFP-Plin3-β and eGFP-Plin3 signal localizing to LDs when expressed alone in Huh7 cells. The insert squares indicate localization region of corresponding protein to the LD surface. Under the same settings, eGFP-Plin3-β always displayed more important signals around LDs than eGFP-Plin3. Scale bar, 10 µm.

(I) The relative bound fraction level of eGFP-Plin3-β co-expression with mCherry-FL Plin3 (shown in figure 2I) is reported and indicates that mCherry FL Plin3 is readily displaced from LDs when coexpressed with eGFP-Plin3-β. ~~GFP/mCherry does not affect the behaviour of the constructs.~~ Each experimental dot corresponds to an average of the signal on 10 to 20 LDs.

Figure 2

(A) mCherry-FL Plin1 co-expression and LD colocalization with GFP tagged versions of FL Plin2, of FL Plin3 (B) and of the Plin1 fragments (C, D) in Huh7 cells. The insert squares indicate the colocalization region of corresponding proteins to the LD surface. Scale bar, 10 µm. This experiment was repeated at least three times with more than fifteen cells analysed for each condition. The relative bound fraction level is reported in the right panel and indicates the relative amount of a protein bound to LDs when mCherry-FL Plin1 (the reference protein) is expressed at a given level; it is calculated as follows: [protein]/([protein]+[reference protein]), and represented against [reference

protein]. Each experimental dot corresponds to an average of the signal on 10 to 20 LDs. Scale bar, 10 µm.

(E) The critical concentration of FL Plin1 required for displacing half of the competing proteins is reported. The Plin1-**C** required much more FL Plin1 to be displaced, as compared to FL Plin2,3 or the Plin1-**N**. Results are presented as box-and-whisker plots of the critical concentration assessed from at least three different sets of data. The central box represents the interquartile ranges (25th to 75th percentile), the middle line represents the median and the horizontal lines represent the minimum and the maximum value of observation range. Values are expressed as median ± IR.

(F) Classification of the relative binding strength to the LD surface of Perilipins and fragments thereof based on their recovery rates from FRAP and competition experiments. Plin 2-**C**, labelled with the asterisk, constitutes a particular case as it has a low LD on rate, suggested from co-expression experiments, and a high off rate, observed from FRAP experiment.

(G) mCherry-FL Plin2 co-expression and colocalization with GFP-tagged versions of the Plin1 fragments. Plin2 is not fully displaced by the fragments and displays frequent differential LD enrichment with the fragments. The experiments were repeated twice and three times respectively. Scale bar is 10 µm.

(H) Critical concentrations for the displacement of proteins competing against mCherry-Plin1-**N**, shown in Figure S3H. The Plin2-**N** and Plin3-**N** were displaced by similar concentrations, whereas the Plin1-**C** required considerably more Plin1-**N** to displace it. The Plin2-**C** was barely detected on LDs in this co-expression experiment. Results are presented as box-and-whisker plots of the critical concentration obtained from at least three sets of data.

(I) GFP-Plin3-β (without β-sheets) co-expression and LD colocalization with mCherry-FL Plin3 in Huh7 cells. FL Plin3 is readily displaced from LDs when coexpressed with GFP-Plin3-β. The insert squares indicate the colocalization region of corresponding proteins to the LD surface. In control experiments, GFP-Plin3 did not displace mCherry-Plin3 as observed with GFP-Plin3-β. Right panel shows the intensity profile of each line section drawn in the inset. Signal on LDs is displayed as Peaks; mCherry-Plin3 is almost absent on LDs only when it was co-expressed with GFP-Plin3-β. ~~The relative bound fraction level is reported in the right panel. S~~Far right panel compares

the relative bound fraction of mCherry-Plin3 when co-expressed at similar level with GFP-Plin3 or GFP-Plin3-β. Scale bar, 10 µm.

(J) FRAP analysis of GFP-Plin3-β in Huh7 cell. A representative image sequence is shown with typical recovery kinetic (K). FRAP experiment was repeated three times. Scale bar, 10 µm.

(L) Histogram of characteristic recovery times of FL Plin3 and Plin3-β in individual FRAP experiments. The characteristic recovery times correspond to means ± SD.

Supplementary Figure 3 (related to Figure 2)

(A) Representative images of GFP-FL Plin1 and mCherry-FL Plin2 when co-expressed and analysed with FRAP in Huh7 cells. FRAP image sequences and quantification are shown. The experiments were replicated three times. Scale bar, 10 µm.

(B) Signal recovery over time of Plin1 FL and Plin1-**N** and (C) of FL Plin1 and Plin1-**C** when co-expressed. The experiments were replicated three times.

(D) Histograms of characteristic recovery time for FL Plin1, vs. FL Plin2 and vs. Plin1 fragments deduced from (A, B, C).

(E) mCherry-FL Plin1 co-expression and colocalization with GFP-tagged FL Plin2. Plin1 and Plin2 are enriched on different LD subpopulations. Scale bar, 10 µm.

(F) mCherry-FL Plin3 co-expression and colocalization with GFP-tagged versions of FL Plin2 and Plin1 fragments. Representative images are shown. This experiment was repeated at least two times. Scale bar 10 µm. The fall off level of the experiments are described in the lower panel. Each experimental dot corresponds to an average of the signal on 10 to 20 LDs.

(G) Critical concentrations for FL Plin3 displacement by Plin2 and Plin1 fragments are reported (from (F)), ns. not significant. Results are presented as box-and-whisker plots of the critical concentration. The central box represents the interquartile ranges (25th to 75th percentile), the middle line represents the median and the horizontal lines represent the minimum and the maximum value of observation range. Values are expressed as median ± IR.

(H) mCherry-Plin1-**N** co-expression with GFP-tagged versions of the other fragments of Plins1-3 in Huh7 cells. The insert squares are zoomed in images of LDs. Scale bar, 10 µm. The bound fraction level is reported in the right panel and indicates the amount

of the mCherry-Plin1-**N** (the reference protein) required to displace the 'competing' protein from the LD surface. Scale bar, 10 µm.

(I) mCherry-Plin2-**C** co-expression and colocalization with the GFP-Plin3-**N** or GFP-FL Plin3; and GFP-Plin2-**C** co-expression and colocalization with the mCherry-Plin1-**N**. Representative images are shown and the experiment was repeated twice. Scale bar 10 µm. The 4HB region of Plin2 is readily displaced from LDs when coexpressed with the other proteins that localise to LDs.

Figure 3

(A) Schematic illustration of perilipin binding to LDs. The FL protein contains a membrane binding domain and a second soluble domain that potentially interacts with the membrane, which would slow down diffusion and the fall off rate.

(B) Schematic illustration of the in vitro system. Purified LDs in buffer are mixed with triolein to generate buffer-in-oil emulsion droplets. LD protein content is relocated in this manner to the resulting oil-water interface.

(C) Schematic illustration of the lateral mobility of the proteins studied by photobleaching.

(D) Schematic illustration of membrane fall off in shrinking buffer-in-oil droplets containing two differently labelled proteins at the droplet interface.

(E) Lateral recovery of mCherry-FL Plin1 and GFP-Plin1-**N** at the oil-water interface of an artificial droplet as sketched in (C). Representative image sequences are shown. Scale bar, 30 µm. Mean fluorescence recovery of the bleached drop surface area over time is shown (right). The experiment was reproduced three times and a representative situation is shown.

(F) Representative images of mCherry-FL Plin1 and GFP-Plin1-**N** fall off from the oil-water interface during shrinkage of the artificial drop (as sketched in (D)). Scale bar, 30 µm. Fluorescence intensity profiles (middle) in the equatorial focal plane of the artificial droplet are plotted against the droplet compression factor, (r^2 (time 0) /r^2 (respective time point); r = drop radius). In the far-right panel, the mean ± SD surface/lumen signal during compression is reported. The experiment was reproduced three times and a representative situation is shown.

(G) Lateral recovery rates of mCherry-FL Plin2 or mCherry-FL Plin3 (I) compared to the GFP-Plin1-**N** at the oil-water interface are reported. Representative images are shown. Scale bar, 30 µm. Mean fluorescence recovery on the droplet bleached surface area over time is shown (right). The experiments were reproduced three times for (G) and twice for (I).

(H) mCherry-FL Plin2 or mCherry-FL Plin3 (J) and GFP-Plin1-**N** fall off during shrinkage are shown. Scale bar, 30 µm. Fluorescence intensity profiles are plotted against the drop compression factor (middle). In the far-right panel, the mean surface/lumen signal ± SD during compression is reported. The experiments were reproduced more than 3 times for (H) and at least twice for (J).

Supplementary Figure 4 (related to Figure 3)

(A-B) GFP/mCherry do not affect the behaviour of proteins. GFP-FL Plin1 and mCherry-Plin1-**N** shows similar latteral diffusion (A) and fall off (B) as with the switched tags, seen respectively in Figure 3E and Figure 3F with mCherry-FL Plin1 and GFP-Plin1-**N**. Experiment was repeated three times. For (B), Fluorescence intensity profile during shrinkage is plotted against the droplet compression factor (right panels). In the far-right panel, the mean ± SD surface/lumen signal during compression is reported. Scale bar, 30 µm.

(C-D) FL Plin1 and Plin1-**C** have conserved relative diffusion rates regardless of their GFP or mCherry tags. Experiment was repeated three times. Representative image sequences are shown. Scale bar, 30 µm.

(E) Lateral recovery of mCherry-FL Plin2 against GFP-Plin-**C** at the buffer-in-oil interface is reported. Representative images are shown. Scale bar, 30 µm. Mean fluorescence recovery ± SD on the bleached droplet surface area over time is shown (right). The experiments were repeated twice.

(F) The level of mCherry-FL Plin2 and GFP-Plin1-**C** upon interface shrinkage is shown. Scale bar, 30 µm. Fluorescence intensity profile during shrinkage is plotted against the droplet compression factor (right panels). In the far-right panel, the mean ± SD surface/lumen signal during compression is reported. The experiment was reproduced 3 times.

Figure 4

(A) Schematic illustration of oil droplet tensiometry showing a oil droplet, whose volume can be adjusted, at the end of a J-tube in an aqueous buffer. When added to the buffer, purified peptide reduces surface tension. Shrinking the droplet, reduces its surface area and increases the concentration of surface peptide further altering surface tension and/or forcing the peptide off the surface.

(B) Plin1 11mr-containing domain (amino acids 93-192) wild type (WT, black line) and mutant (L143D, red line) peptides decrease the interfacial tension of a triolein/water (TO/W) interface, but less for the mutant.

(C) Equilibrium surface pressure (π_{eq}) versus the concentration of peptide in the bulk phase. WT produces a higher π (i.e. lower surface tension) than the L143D mutant at all concentrations. At the lowest concentrations (less than 0.5µg/ml) the values may be too low because equilibrium probably had not been reached.

(D) Having reached a stable equilibrium (~16.3 mN/M) following injection of the Plin1 WT peptide, the droplet area (size) was rapidly reduced to produce a surface compression and after a few minutes re-expanded. Changes in surface tension are displayed during this procedure. After the rapid compression, surface tension comes back to the initial equilibrium tension. Data from further compressions is included in Figure S5A.

(E) Competition for the TO/W interface between Plin1 93-192 WT and mutant L143D. Initial (red arrow) addition of 10 µg of mutant L143D to the TO/W interface promptly reduced surface tension to ~18.6 mN/m (γ_{eq}). The area was then reduced by ~30% causing the tension to fall rapidly to ~17.6 mN/m. It then quickly returned to equilibrium. The area was then re-expanded and tension spiked to ~27.1 mN/m before falling back to γ_{eq}. An equivalent amount of Plin1 WT peptide was then also injected within few minutes (+WT arrow) and surface tension slowly fell further to a new γ_{eq} of ~15.6 mN/m, indicating that WT displaced the mutant peptide. The surface tension profile following a repeat compression and re-expansion was somewhat different than that recorded during a similar compression in the presence of mutant peptide alone, insofar as there was a 'shoulder' (arrowhead) in the recovery period – we interpret this as reflecting initial rapid re-association of both mutant and WT peptides with the interface but then over time, the mutant is entirely displaced by the WT peptide.

(F) This image is similar to Figure 4D but here phospholipid (POPC) has been added to the buffer prior to addition of Plin1 WT peptide and then a compression/re-expansion perturbation. Note that the equilibrium surface tension is lower when POPC is added

i.e. ~ 13.6 mN/m. After the rapid compression, the new equilibrium surface tension is lower than the initial equilibrium tension, conversely to 4D. Data from further compressions for both the WT and L143D mutant peptide is included in Figure S5B.
(G, H) The maximum pressure the peptide can withstand without being ejected from the interface is referred to as Π_{max}. Data from a number of rapid compression experiments plotting the maximum Π (Πo) obtained for a given compression is plotted against the change in ($\Delta\gamma$) after compression. The extrapolations to $\Delta\gamma = 0$ give Π_{max} for each peptide on the two interfaces. G, The Π_{max} for the WT peptide is shown for the TO/W and POPC/TO/W interfaces. Π_{max} is higher on the POPC/TO/W interface suggesting that the presence of POPC helps to retain the peptide at the interface. Exclusion pressure is calculated by extrapolating the regression lines to a surface tension increment of zero. These data are reported in H.

Supplementary Figure 5 (related to Figure 4)
(A) (left panel) Schematic illustration of the interaction of peptides with a naked triolein-buffer interface. (right panel) The effect of Plin1 (amino acids 93-192) wild type (WT, black line, upper panel) and mutant (L143D, red line, lower panel) peptides on the interfacial tension of a triolein/water (TO/W) interface. The same initial data is shown in Figure 4B, but here the data for several subsequent compression/ re-expansion cycles is included.
(B) (left panel) Schematic illustration of the oil droplet with both phospholipid (POPC) and peptide added. (right panel) The effect of WT (black line, upper panel) and L143D mutant (red line, lower panel) peptide addition to a TO/W/POPC interface on surface tension before and after several surface compressions. Here we also include data following 'washout' of the residual peptide in the buffer. In this case, each compression is associated with net loss of peptide so the equilibrium surface tension rises progressively back towards the initial surface tension following addition of POPC alone.
(C) Competition for the POPC/TO/W interface between Plin1 93-192 WT and mutant L143D. Initial addition of phospholipid (+POPC arrow) to the buffer slowly reduced surface tension to ~ 26 mN/m (γ_{eq}). POPC in the aqueous phase was removed by washout. Following addition of 10 μg of mutant L143D (+L143D arrow) to the buffer, surface tension promptly fell to ~17.3 mN/m(γeq). The area was then reduced by ~30% causing the tension to fall rapidly before returning to a lower surface tension of ~15-16

mN/m. The area was then re-expanded and tension spiked before falling back to γeq. An equivalent amount of Plin1 WT peptide was then also injected (+WT arrow) and surface tension slowly fell to a new γ_{eq}. of ~14.7 mN/m indicating that WT displaced the mutant peptide. The surface tension profile following a repeat compression and re-expansion was somewhat different to that recorded during a similar compression in the presence of mutant peptide alone, insofar as there was a 'shoulder' (similar to that seen on the TO/W interface (see Figure 4E)) in the recovery period – we interpret this as reflecting initial rapid re-association of both mutant and WT peptide with the interface but then over time, the mutant is entirely displaced by the WT peptide.

(D,E) The maximum pressure the peptide can withstand without being ejected from the interface is referred to as Π_{max}. Data from a number of rapid compression experiments plotting the maximum Π (Π_0) obtained for a given compression is plotted against the change in (Δγ) after compression. The extrapolations to $\Delta\gamma = 0$ give Π_{max} for each peptide on the two interfaces. (D) The Π_{max} for the WT (black) and L143D mutant (red) peptide is shown for the TO/W interfaces. Π_{max} was consistently higher for the WT than for the mutant peptide. (E) Similarly to the Plin1 WT peptide (Figure 4G), the Π_{max} for the L143D mutant was consistently higher in the presence of POPC (green circles) than in its absence (red). Values for Π_{max} are summarized in Figure 4H.

METHOD DETAILS

Cloning of Plin1-3 and peptide fragments

Human cDNAs encoding full length Plin1 (aa 1-522), Plin2 (aa 1-437) and Plin3 (aa1-434) were PCR amplified using Phusion DNA polymerase (Thermofisher) from the templates pcDNA-Myc Plins1-3 (Patel 2014) and subcloned in frame into pEGFPC1 (Clontech) or pMCherry. The cDNAs encoding the fragments for Plin1 (aa1-191 and aa185-522), Plin2 (aa1-191 and aa 184-437) and Plin3 (aa1-204 and 197-434) were PCR amplified from the pcDNA Plins1-3-Myc (Rowe et al., 2016) and also subcloned into pEGFCPC1 and pMCherry. The restriction endonucleases employed for the Plin1-3 subcloning strategies are as follows HindIII/Sal1 for Plin1, EcoR1/Sal1 for Plin2 and EcoR1/BamH1 for Plin3. Plin3-ß (aa1-413) were amplified by PCR from the template pEGFP Plin3 and subcloned into pEGFPC1. All Plin constructs were cloned such that the GFP or mCherry fluorescent tag was N-terminal to the gene and thus peptide or protein.

Expression and purification of the Plin1 11-mer repeat region

Recombinant plasmids pET22b-CPD-SalI expressing perilipin1 amino acids (93-192) were transformed into the E.coli expression strain NiCo21 (New England Biolabs, Hitchin, UK). The L143D Plin1 mutant peptide was generated as described previously (Rowe et al., 2016). Overnight cultures were diluted into 1 liter of lysogeny broth supplemented with 0.2% glucose and grown with shaking at 37 °C to A600 = 1.0. Isopropyl-D-1-thiogalactopyranoside was added (1 mM final concentration) and cultures were further grown for 80 min at 37 °C. Cell pellets from a 500-ml culture were resuspended in 14 ml of B-PER (Thermo Scientific) with 10% glycerol, 4 mg of lysozyme (Sigma), 500 units of Pierce Universal Nuclease (Thermo Scientific) and complete EDTA-free protease inhibitors (Roche Applied Science). Cell lysates were rotated at room temperature for 15 min, to ensure full cell lysis, centrifuged at 28,000 x*g* for 30 min and filtered (Minisart 0.22 μm; Sartorius, Göttingen, Germany). Affinity purification was performed using 0.5–1.0 ml of nickelnitrilotriacetic acid-agarose beads (Qiagen) while rotating for 1 h at 4 °C, before bound fusion proteins were subjected to high stringency washes (40mM imidazole, 0.5M NaCl) to reduce non-specific protein binding and transferred to the CPD reaction buffer (20mM Tris, 60mM NaCl, 250mM sucrose, 3mM imidazole, pH 7.4). Cleaved products were eluted into the supernatant

using 50–100μM inositol hexakisphosphate by gentle rotation for 2 h at 4 °C. Size exclusion chromatography was performed using an AKTA pure chromatography system and SuperdexTM 75 10/300 GL column (GE Healthcare). Protein concentrations were determined by amino acid analysis. To confirm ≥95% purity, equivalent amounts of isolated proteins were resolved on an 18% Tris-glycine gel (Life Technologies, Inc.) and stained with quick Coomassie stain (Generon, Maidenhead, UK). The purified proteins were analysed by mass spectrometry (LC-MS) revealing a 90 amino acid peptide sequence and apparent mass of approximately 9400 daltons. We were able to distinguish the wildtype from the mutant L143D peptide based on retention time and mass profile. We also identified a cryptic cleavage site close to the C-terminus which removed amino acid residues 181-192 from the intact peptide. Further dynamic light scattering studies (0.5mg/ml protein samples in 10mM potassium phosphate buffer pH 7.4) using a Zetasizer NanoS instrument (Malvern Ltd, UK) showed negligible levels of aggregation and confirmed earlier findings that these proteins were essentially monomeric by the initial gel filtration elution profile (data not shown).

Cell Culture.

Huh7 cells were maintained in Dulbecco's modified Eagle's medium (DMEM) supplemented with 10% heat inactivated fetal bovine serum (Life Technologies), 4.5 gL^{-1} D-glucose, 0.1 gL^{-1} sodium pyruvate (Life Technologies) and 1% penicillin-streptomycin (Life Technologies). The cells were cultured at 37°C under a 5% CO2 atmosphere. Confluent monolayers of cells were re-suspended after trypsinization and plated into a 35 mm cell-culture Mattek dishes (with a glass coverslip at the bottom), (MatTek Corp. Ashland, MA).

HeLa (human cervical carcinoma obtained from ATCC) cells were maintained in Dulbecco's Modified Eagle's Medium supplemented with 10% (vol/vol) fetal bovine serum (FBS), 2 mM L-glutamine, penicillin/streptomycin, 1 % Sodium Pyruvate, 1 % Non-Essential Amino Acids.

Transfection and co-transfection.

When indicated Huh7 cells (60-70% confluence) were exposed for 1hr to 500 μM oleic acid coupled to BSA (1% v:v) to induce LD formation and then cells were transfected with 3 μg of plasmid DNA/mL using Polyethylenimine HCl MAX (Polysciences, Inc)

following the manufacturer's instructions. For co-expression competition experiments, mCherry- or GFP-tagged plasmid constructs in equal concentrations (1.5-2 µg for each one) were transfected into cells. 24 hrs after transfection, cells were imaged.
HeLa cells were seeded onto coverslips in 12 well tissue culture plates with a density of 65,000 cells per well and transfected using Lipofectamine LTX (Thermo Fischer Scientific). 400 µM oleic acid conjugated to BSA, along with either Bodipy 558/568 C_{12} or 493/502 (1:2500 dilution), was supplemented 4 hours after transfection for 20 hrs to promote lipid droplet formation and staining. Cells were fixed with 4 % formaldehyde for 15 mins, followed by three washes in PBS. Cells were mounted on microscope slides with ProLong Gold Antifade Mountant with DAPI (Thermo Fischer Scientific) and the fluorescently-tagged protein localization was determined using the Leica TCS SP8 confocal microscope with a 63X immersion oil objective (1.3 NA). Green fluorescent protein fluorescence was excited at 488 nm and emission was detected between 490 and 550 nm, whilst m-cherry-tagged protein fluorescence excited at 588 and emission detected between 600 and 650 nm. Lipid droplets were detected with either Bodipy 493/502 (excitation – 502 nm, emission 515-560 nm) or Bodipy 558/568 C_{12} (excitation – 558 nm, emission 590-700 nm).

FRAP experiments

For FRAP experiments, we bleach the signal on a collection of drops and monitor the increase of signal during recovery. The background signal, e.g. from the cytosol, is removed from the recorded signal, which was at the end normalized by intrinsic bleaching of non-bleached areas. We next used GraphPad Prism to fit the FRAP recovery curves with a non-linear regression and the exponential « one-phase association model ». The characteristic recovery time that corresponds to the time it takes for fluorescence intensity to reach half the maximum of the plateau level is obtained by the software.

Image Quantification and Statistics

Images were analyzed using ImageJ software. For quantification of the % LD-targeted signal for a given protein, the image was background corrected and the total fluorescent signal on LDs was determined as a ratio to the total fluorescent signal in the whole cell. In co-expression experiments, the fluorescence signal on LDs was calculated by

subtracting out the fluorescence signal elsewhere in each cell. Protein concentrations on LDs were derived from the mean fluorescence measured on LDs in each channel; each experimental point shown in figures 2-3 corresponds to the average of the signal on 10 to 20 LDs. Values from 15–20 cells were combined, and the standard deviation was calculated for statistical analysis. The critical concentration was determined by fitting the data with the following function: $y = 1/(1+x/c)$, where c represents the critical concentration at which half of the competing protein is displaced.

In vitro experiments

To purify LDs from cells expressing fluorescently tagged LD proteins, cells from 5 150-cm dishes were harvested, washed once in ice-cold PBS, and lysed using a 30G needle in 1ml Tris-EDTA (20 -10 mM) buffer containing complete protease and phosphatase inhibitor tablets at pH 7.5. To isolate LDs, 1ml cell lysates were mixed with 1 ml of 60% sucrose in Tris-EDTA buffer supplemented with protease inhibitors, overlaid with 20%, 10% and 0% in buffered sucrose on top of one another in 5 ml Ultra-Clear centrifuge tubes (Beckman). Gradients were centrifuged for 16 h at 100 .000x*g* and 4 °C, using an SW60 rotor in a Beckman L8-70 centrifuge, and 300 µL were collected from the top as the LD fraction.

In vitro experiments were performed in HKM buffer: 50 mM Hepes, 120 mM Kacetate, and 1 mM $MgCl_2$ (in Milli-Q water) at pH 7.4. To create buffer-in-oil drops, 4 µL of a buffer-diluted LD fraction was mixed with 40 µL of triolein by vortexing to create buffer-in-oil drops, as previously done (Kory et al., 2015). About a hundred drops are formed and imaged in the field of observation. For shrinking experiments, aqueous drops bounded by the proteins were imaged for 10 to 30 min, on glass plates, during water evaporation. For the diffusion experiments, we bleached part of the droplet surface and the fraction of recoverable fluorescence was calculated with respect to initial fluorescence.

Lipids

Triolein (TO) was purchased from Nu-Chek Prep, Inc. (Elysian MN). It was > 99% pure and its interfacial tension at 25.0ºC was 32 ± 1 mN/m. POPC (palmitoyloleoyl phosphatidylcholine) from Avanti Polar Lipids (Alabaster AL) was stored at -20ºC in chloroform (25.0mg/ml). Small ~ 30 nm POPC unilamellar vesicles (SUV at 2.5

mg/ml) were formed in standard 5mM sodium phosphate buffer (pH7.4) by sonication as previously described (Meyers et al., 2013; Mitsche et al., 2010).

Interfacial tension (γ) and surface pressure (π) measurements

We modified an oil-drop tensiometer (Meyers et al., 2013; Mitsche and Small, 2013; Mitsche et al., 2010) designed by Teclis Instruments (Tassin, France) to measure the interfacial tension (γ) of lipid/water interfaces. γ is the energy required to create one new cm^2 of surface (i.e., γ = ergs/cm^2 or mN/m). All experiments were conducted at 25.0±0.2ºC in a thermostated system and repeated at least twice.

To create triolein/water (TO/W) interfaces (Mitsche and Small, 2011), triolein drops (16.0µl) were formed at the tip of a J-needle submerged in 7.0ml of bulk buffer. Their surface area was ~ 30mm^2 (diameter =3.1 mm). The buffer was 5 mM sodium phosphate at pH 7.4. Prior to interfacial studies, aliquots of the wildtype and mutant Plin1 peptides were thawed and solubilized with hexafluoro-2-proponol (HFIP) at a concentration of 2.5% (V/V). The TO/W interface stabilized at γ_{TO} = 32.0±1mN/m. Adsorption of amphipathic molecules (i.e. phospholipid, Plin peptides) to this interface shields much of the TO from the aqueous phase and decreases γ to a nearly constant value defined as equilibrium tension (γeq). To create POPC/TO/W interfaces, triolein drops of 16µL were formed in bulk buffer containing 1.0 mg of POPC SUV. After POPC adsorbed to the triolein drop, the buffer was exchanged with 250 ml of POPC-free buffer, originally described for egg yolk PC (Mitsche et al., 2010) to washout > 99.9% of the original buffer and all POPC SUVs suspended in the bulk phase. After a washout, γ was usually usually 25-27 mN/m corresponding to about 1.1 µmols POPC/m2 for POPC/TO/W interfaces. Varied amounts of Plin1 peptide were added to the bulk phase to obtain different protein concentration ranging from 0.2 to 4µg/mL. As peptide adsorbed to TO/W and POPC/TO/W interfaces, γ was monitored continuously as it fell to an equilibrium value (γ_{eq}). Surface pressure (Π) was defined as the difference in γ between a pure TO/W interface (γ_{TO} =32.0 mN/M) and the interface with bound POPC and/or peptide ($\Pi = \gamma_{TO} - \gamma$). The initial pressures (Π_i) of POPC/TO/W interfaces represent the difference between γ_{TO} and γ after POPC adsorption ($\Pi_i = \gamma_{TO} - \gamma_{POPC}$) and was between 5 and 7mN/m. Π_i of the TO/W interface was 0 mN/m. After peptide adsorption, the equilibrium pressure of all interfaces was calculated as $\Pi_{eq} = \gamma_{TO} - \gamma_{eq}$. The change in pressure (ΔΠ) at these interfaces induced by adsorption was $\Delta\Pi = \Pi_{eq} - \Pi_i$.

Pressure/Area mediated Desorption and Readsorption Processes

Following adsorption of peptide to either a TO/W or a POPC/TO/W interface, the drop underwent a series of compressions and re-expansions with the goal of determining if peptide completely or only partially desorbed from the respective interface. Once γ approached a γ_{eq} the TO drop (16 µl) was compressed by rapidly decreasing the volume by different ratios: 6.25% (1 µl), 12.5% (2 µl), 25% (4 µl), 37.5% (6 µl), 50% (8 µl), or when possible, 62.5% (10 µl). This sudden decrease in volume induced a decrease in drop surface area, resulting in a sudden compression and abrupt decrease in γ. The oil drop was held at this reduced volume for 5-10 min, with γ recorded continuously. If peptide readily desorbed, γ increased to a γ_{eq} observed as a desorption curve. After 5-10 min, the interface was expanded by increasing the volume of the drop back to its initial volume (16 µl). As the surface area increased upon expansion, γ abruptly increased. If peptide adsorbed from the bulk phase and adhered to the newly formed extra surface, γ decreased to the initial γ_{eq} observed as a readsorption curve. This process of stress compression and re-expansion was repeated after the bulk buffer was exchanged with 150 mL of 5 mM PB (pH 7.4) devoid of peptide.

Values of $\prod_{max}$

The desorption and readsorption protocol provided information about not only the nature of ejection of the peptide from either interface but also the ∏ at which such ejection occurs. $\prod_{max}$ is the maximal pressure (∏) that a peptide can withstand before all or part of the molecule is ejected from the surface. Once a γ_{eq} had been reached following adsorption of peptide to TO/W or POPC/TO/W interface, a series of experiments were conducted in which the drop Area was decreased abruptly, thereby decreasing γ and increasing ∏ to a given value, $\prod_o$. The change in tension (Δγ) over the following 5-10 min as peptide desorbed from the surface was plotted against $\prod_o$. Regression of a linear fit to the plot reveals $\prod_{max}$ as the point at which Δγ = 0, such that no peptide desorbs from the surface upon compression.

Exclusion pressure (Π_{EX}) measurements

Exclusion pressure (Π_{EX}) for each variant is the surface pressure above which that peptide cannot bind and insert into POPC/TO/W interfaces (Mitsche et al., 2010). In

other words, Π_{EX} is the pressure of a POPC/TO/W interface at which addition of peptide to the bulk phase leads to no adsorption-induced change in surface pressure ($\Delta\Pi = 0$ mN/m)).

Supplementary text: Lateral diffusion model

Diffusion of a particle is limited by dragging forces, which express $f \sim \mu v d$, where μ represents the fluid viscosity, v is the particle speed, and d is the particle diameter. For a molecule at an oil/water (o/w) interface, the forces exerted on the molecule at the aqueous and oil phase determine its lateral diffusion. The contribution of the water force to diffusion can be neglected when $\mu_w v d_w \ll \mu_o v d_o$, which means that $\mu_w/\mu_o \ll d_o/d_w$. Here, this condition is respected as the gyration radius of the soluble helix bundle and the 11mrs are comparable, $d_o/d_w \sim 1$, while indeed the viscosity of water (cP) is much lower than that of triolein (50cP), $\mu_w/\mu_o \sim 0.02$. When the helix bundle in the full length protein interacts with the oil/water interface, in addition to the 11mr, the overall dragging force in the oil is higher that when the 11mrs alone binds; diffusion is then slowed down.

Quantification and statistical analysis

The data of the critical concentrations for displacing competing proteins experiments are presented using Tukey box-and-whisker plots, where the central box represents the interquartile ranges (IR; 25th to 75th percentile), the middle line represents the median, and the horizontal lines represent the minimum and the maximum values of the observation range. Values are expressed as median±IR.

The statistical evaluation of FL Plin3 displacement from LDs by the Plin1 11 mer-repeat or FL Plin2 (in Figure S3G) was done with a Mann–Whitney non-parametric test using prism software, P-values <0.05 were considered significant. All values shown in the text and figures are mean ± SD, where N = 4, from independent experiments.

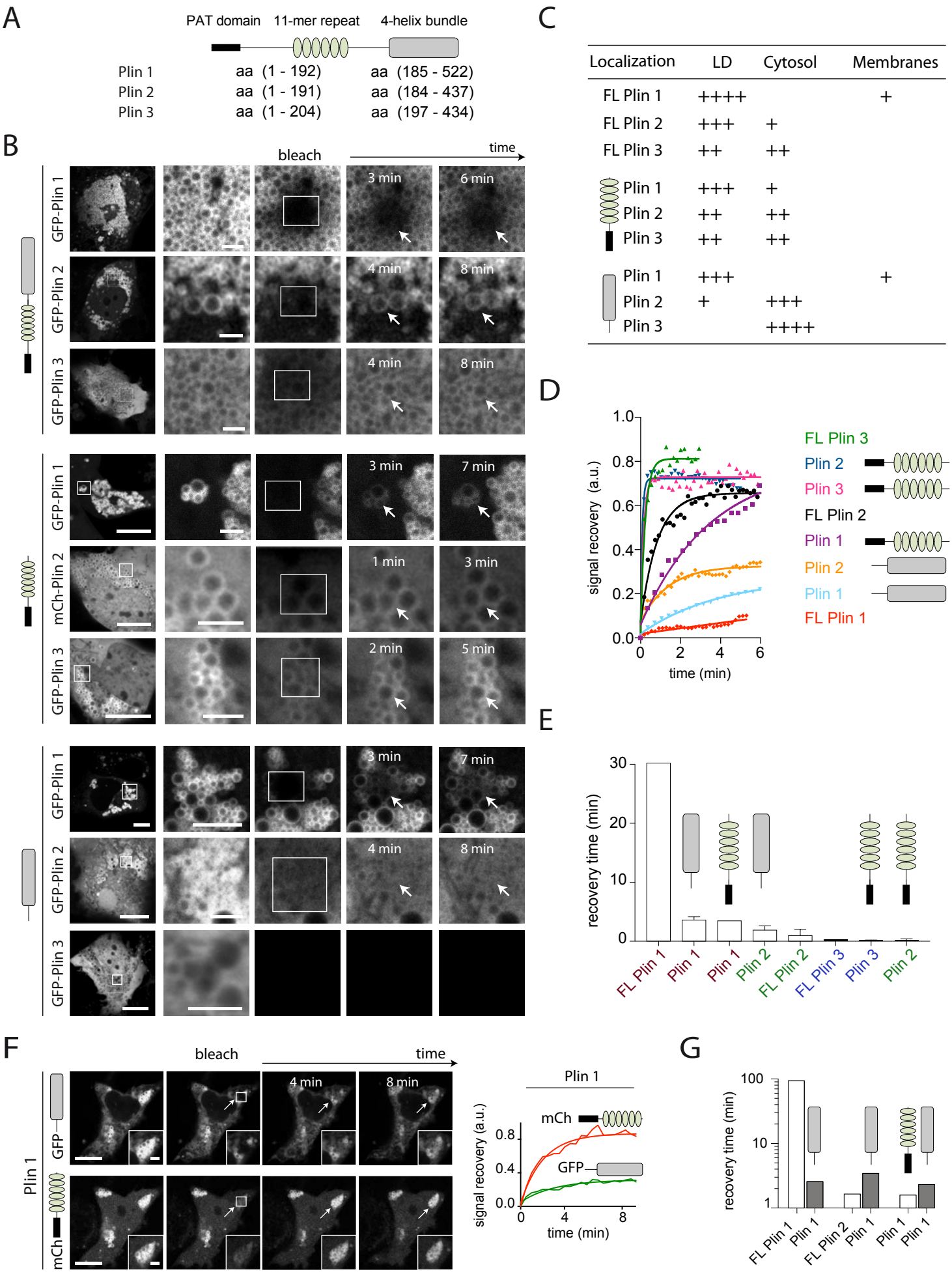
A
PAT domain
11-mer repeat
4-helix bundle
Plin 1 aa (1 - 192) aa (185 - 522)
Plin 2 aa (1 - 191) aa (184 - 437)
Plin 3 aa (1 - 204) aa (197 - 434)
B
bleach
time
GFP-Plin 1
GFP-Plin 2
GFP-Plin 3
mCh-Plin 2
3 min
4 min
6 min
7 min
8 min
1 min
2 min
5 min
C
Localization
LD
Cytosol
Membranes
FL Plin 1 ++++ +
FL Plin 2 +++ +
FL Plin 3 ++ ++
Plin 1 +++ +
Plin 2 ++ ++
Plin 3 ++ ++
Plin 1 +++ +
Plin 2 + +++
Plin 3 ++++
D
signal recovery (a.u.)
time (min)
FL Plin 3
Plin 2
Plin 3
FL Plin 2
Plin 1
Plin 2
Plin 1
FL Plin 1
E
recovery time (min)
FL Plin 1
Plin 1
Plin 1
Plin 2
FL Plin 2
FL Plin 3
Plin 3
Plin 2
F
bleach
time
Plin 1
GFP
mCh
4 min
8 min
Plin 1
mCh
GFP
signal recovery (a.u.)
time (min)
G
recovery time (min)
FL Plin 1
Plin 1
FL Plin 2
Plin 1
Plin 1
Plin 1

Figure 1

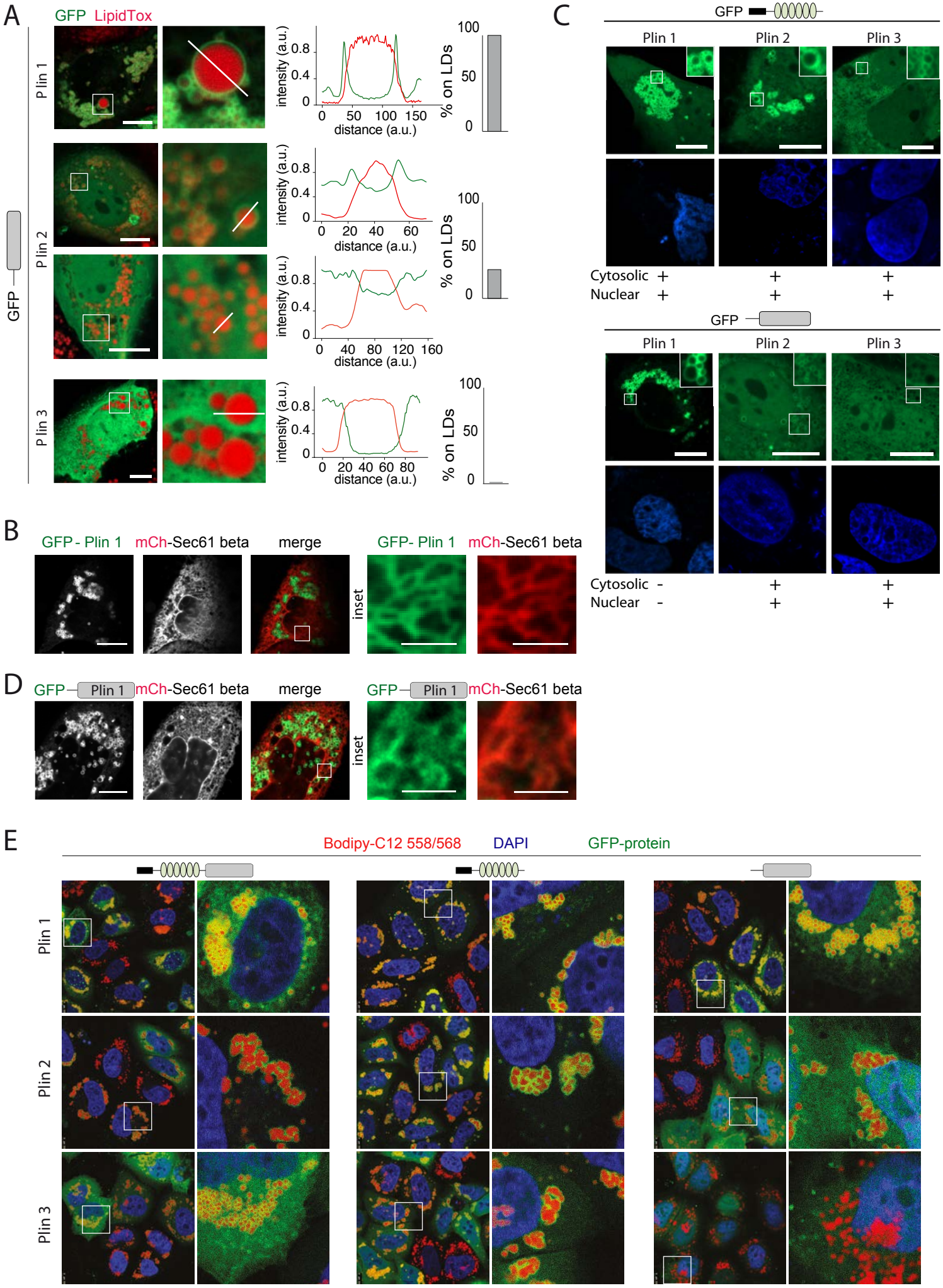
A
GFP LipidTox
P lin 1
P lin 2
P lin 3
GFP
intensity (a.u.)
distance (a.u.)
% on LDs
B
GFP - Plin 1
mCh-Sec61 beta
merge
inset
C
GFP
Plin 1
Plin 2
Plin 3
Cytosolic + + +
Nuclear + + +
Cytosolic - + +
Nuclear - + +
D
GFP Plin 1 mCh-Sec61 beta
merge
inset
E
Bodipy-C12 558/568
DAPI
GFP-protein
Plin 1
Plin 2
Plin 3

Figure 1S

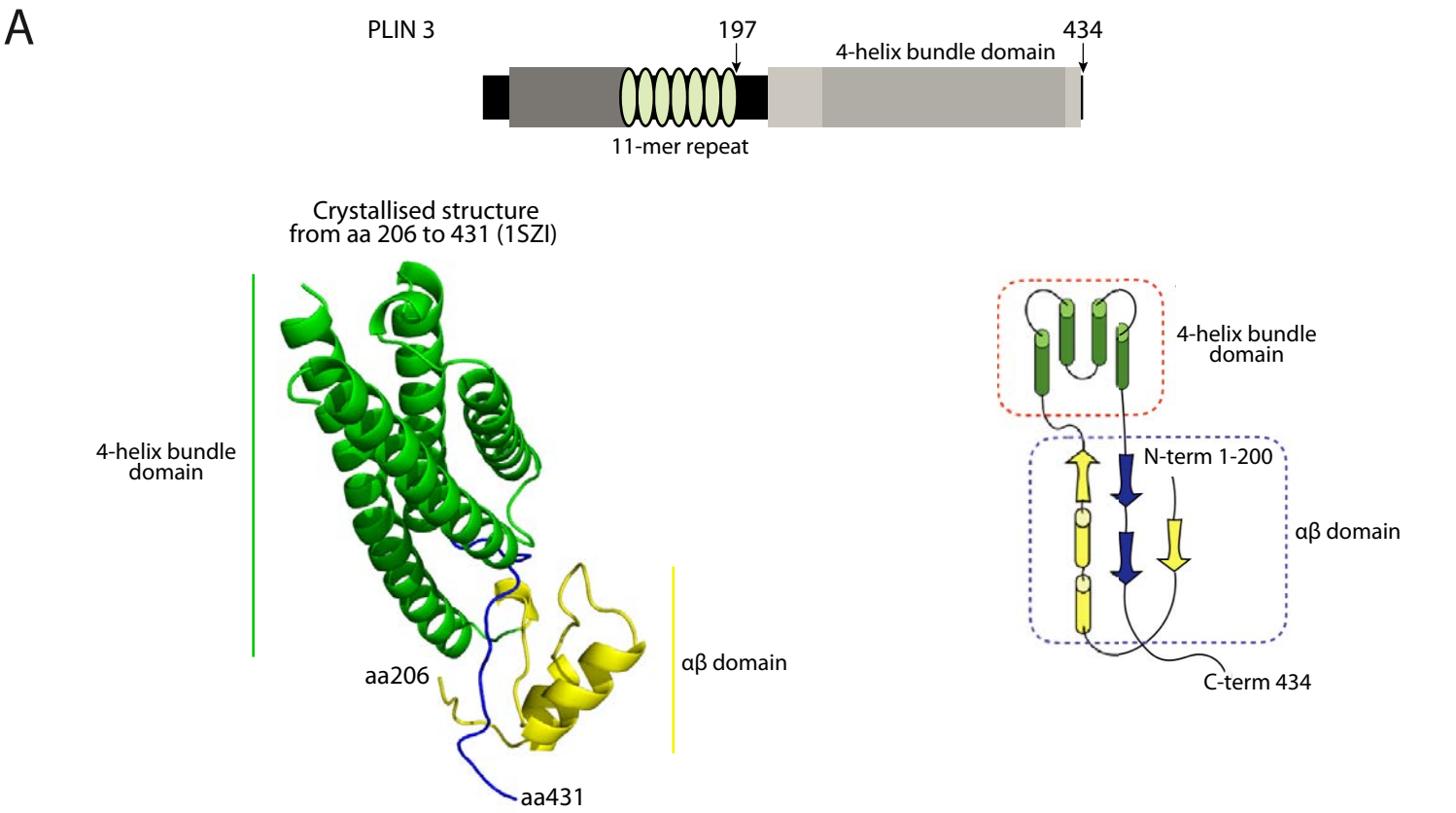

B

1szi	205	D	N	R	L	P	L	210	237	Q	N	Y	F	V	R	L	G	244	417	P	A	M	W	L	V	G	P	F	A	P	G	428
Plin1	189	E	Y	L	L	P	A	194	216	P	S	L	L	S	R	V	G	223	403	P	L	P	R	L	S	L	M	E	P	E	S	414
Plin2	187	E	Q	Y	L	P	L	192	213	P	S	Y	Y	V	R	L	G	220	396	P	L	N	W	L	V	G	P	F	Y	P	Q	407
Plin3	201	D	N	H	L	P	L	206	233	Q	S	Y	F	V	R	L	G	240	413	P	V	T	W	L	V	G	P	F	A	P	G	424
Plin4	1146	D	I	F	H	P	M	1151	1174	G	S	Y	F	V	R	L	G	1181	1341	P	L	S	W	L	V	G	P	F	A	L	P	1352
Plin5	163	D	H	F	L	P	M	168	195	Q	G	Y	F	V	R	L	G	202	370	P	L	P	W	L	V	G	P	F	A	P	I	381

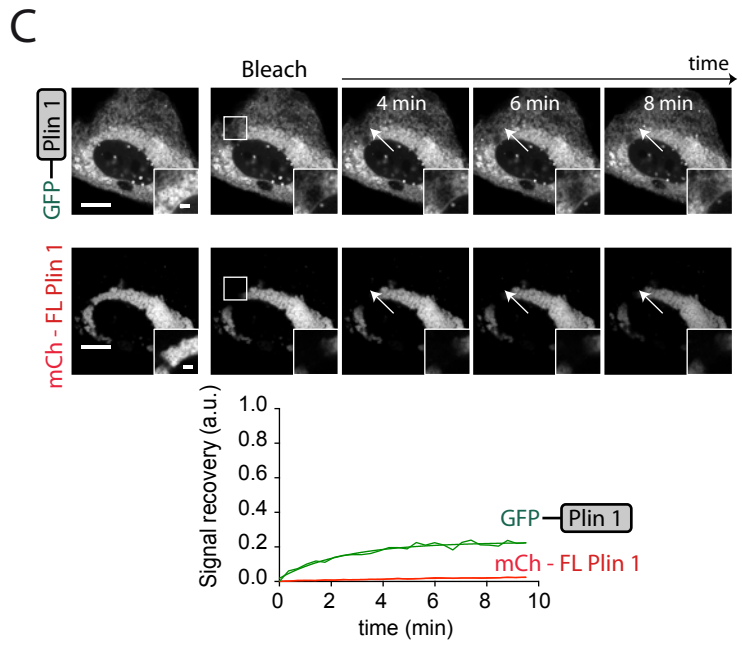

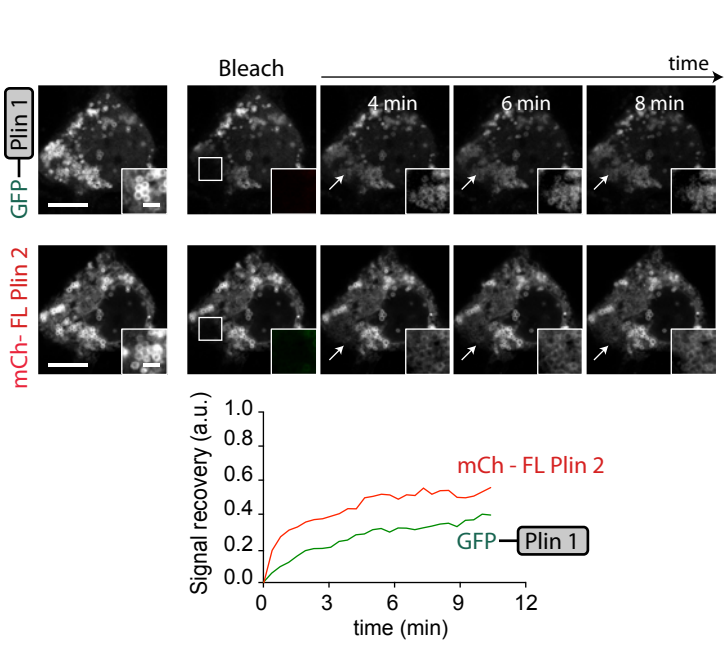

Figure 2S

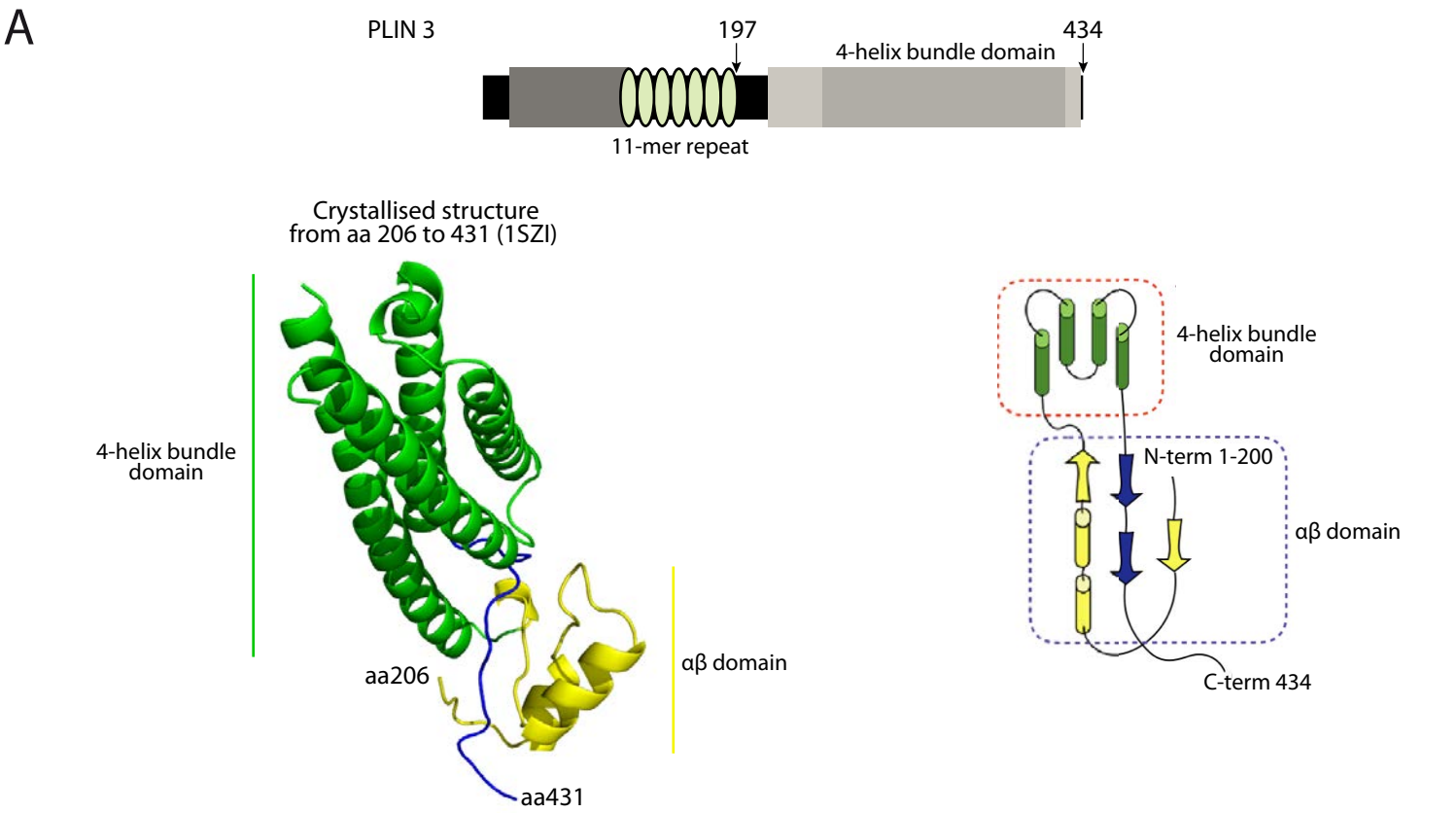

B

1szi	205	D	N	R	L	P	L	210	237	Q	N	Y	F	V	R	L	G	244	417	P	A	M	W	L	V	G	P	F	A	P	G	428
Plin1	189	E	Y	L	L	P	A	194	216	P	S	L	L	S	R	V	G	223	403	P	L	P	R	L	S	L	M	E	P	E	S	414
Plin2	187	E	Q	Y	L	P	L	192	213	P	S	Y	Y	V	R	L	G	220	396	P	L	N	W	L	V	G	P	F	Y	P	Q	407
Plin3	201	D	N	H	L	P	L	206	233	Q	S	Y	F	V	R	L	G	240	413	P	V	T	W	L	V	G	P	F	A	P	G	424
Plin4	1146	D	I	F	H	P	M	1151	1174	G	S	Y	F	V	R	L	G	1181	1341	P	L	S	W	L	V	G	P	F	A	L	P	1352
Plin5	163	D	H	F	L	P	M	168	195	Q	G	Y	F	V	R	L	G	202	370	P	L	P	W	L	V	G	P	F	A	P	I	381

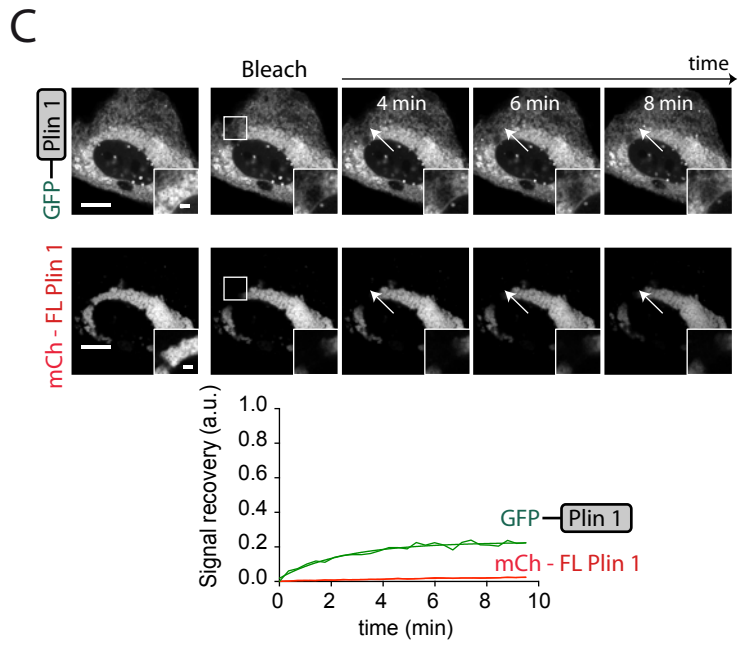

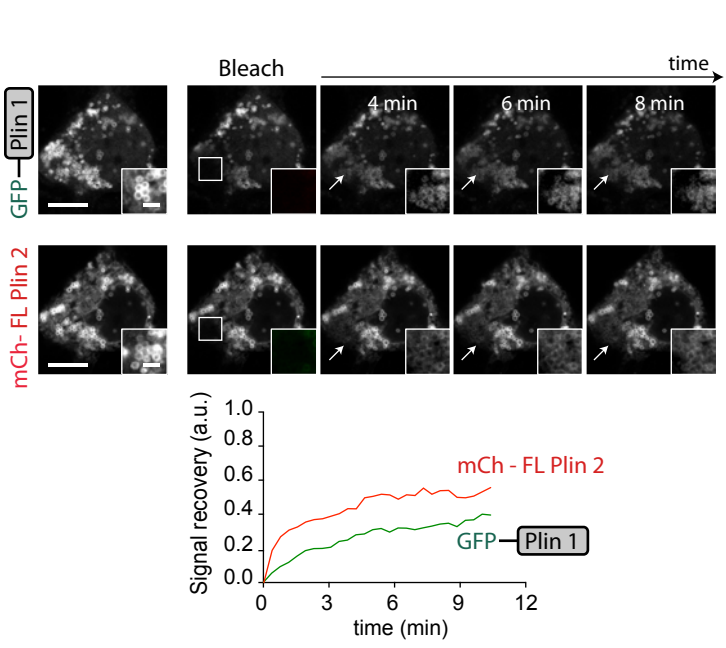

Figure 2S

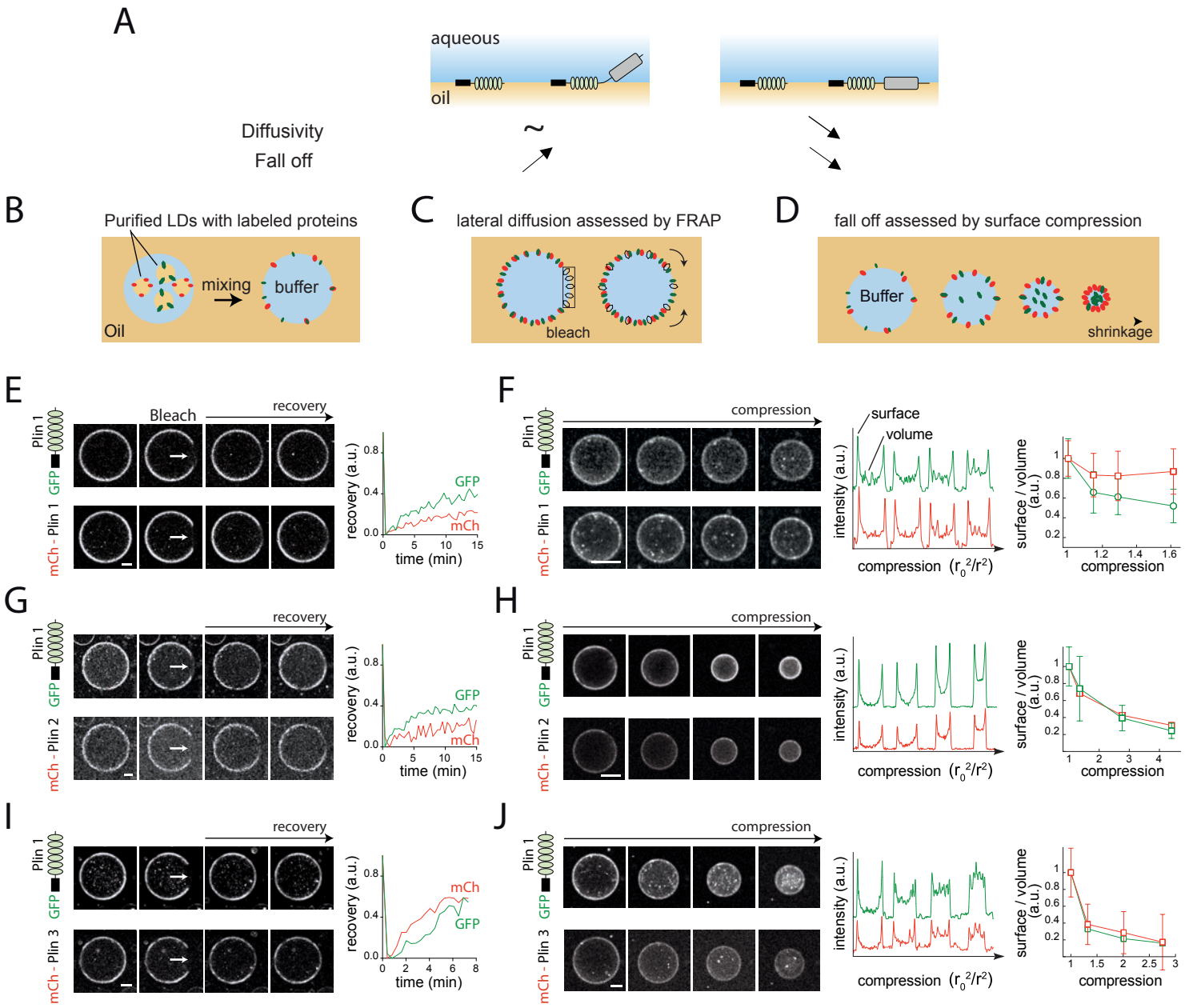
A
aqueous
oil
Diffusivity
Fall off
B
Purified LDs with labeled proteins
mixing
buffer
Oil
C
lateral diffusion assessed by FRAP
bleach
D
fall off assessed by surface compression
Buffer
shrinkage
E
Bleach
recovery
Plin 1
GFP
mCh - Plin 1
recovery (a.u.)
time (min)
F
compression
surface
volume
intensity (a.u.)
compression (r0²/r²)
surface / volume (a.u.)
G
mCh - Plin 2
H
I
mCh - Plin 3
J

Figure 3

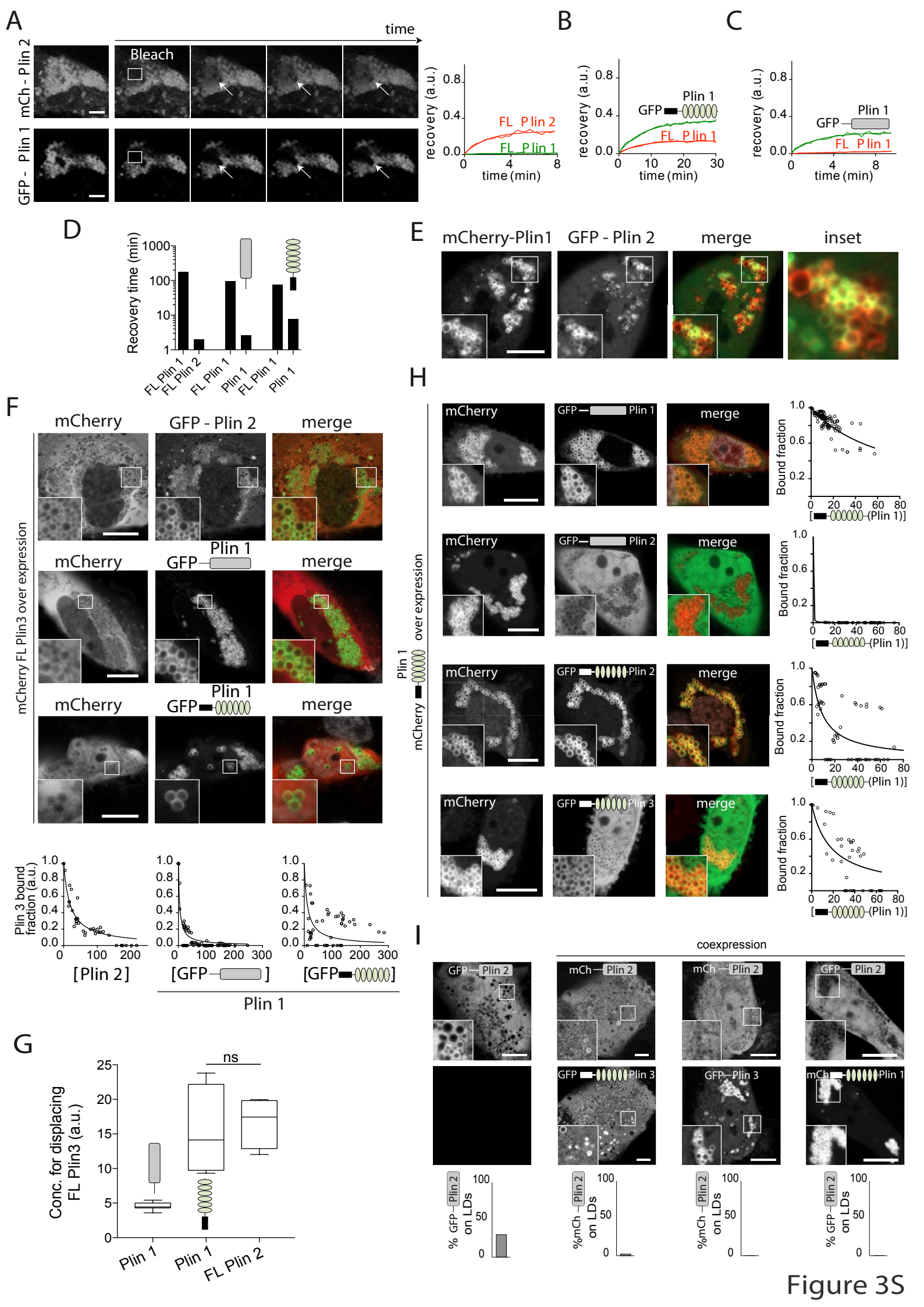
A
time
Bleach
mCh - Plin 2
GFP - Plin 1
recovery (a.u.)
FL Plin 2
FL Plin 1
time (min)
B
Plin 1
GFP
C
D
Recovery time (min)
FL Plin 1
FL Plin 2
Plin 1
E
mCherry-Plin1
GFP - Plin 2
merge
inset
F
mCherry
GFP - Plin 2
Plin 1
mCherry FL Plin3 over expression
Plin 3 bound fraction (a.u.)
[Plin 2]
[GFP]
Plin 1
G
Conc. for displacing FL Plin3 (a.u.)
ns
H
Plin 1 over expression
mCherry
Bound fraction
(Plin 1)
I
coexpression
mCh
% GFP Plin 2 on LDs
%mCh Plin 2 on LDs

Figure 3S

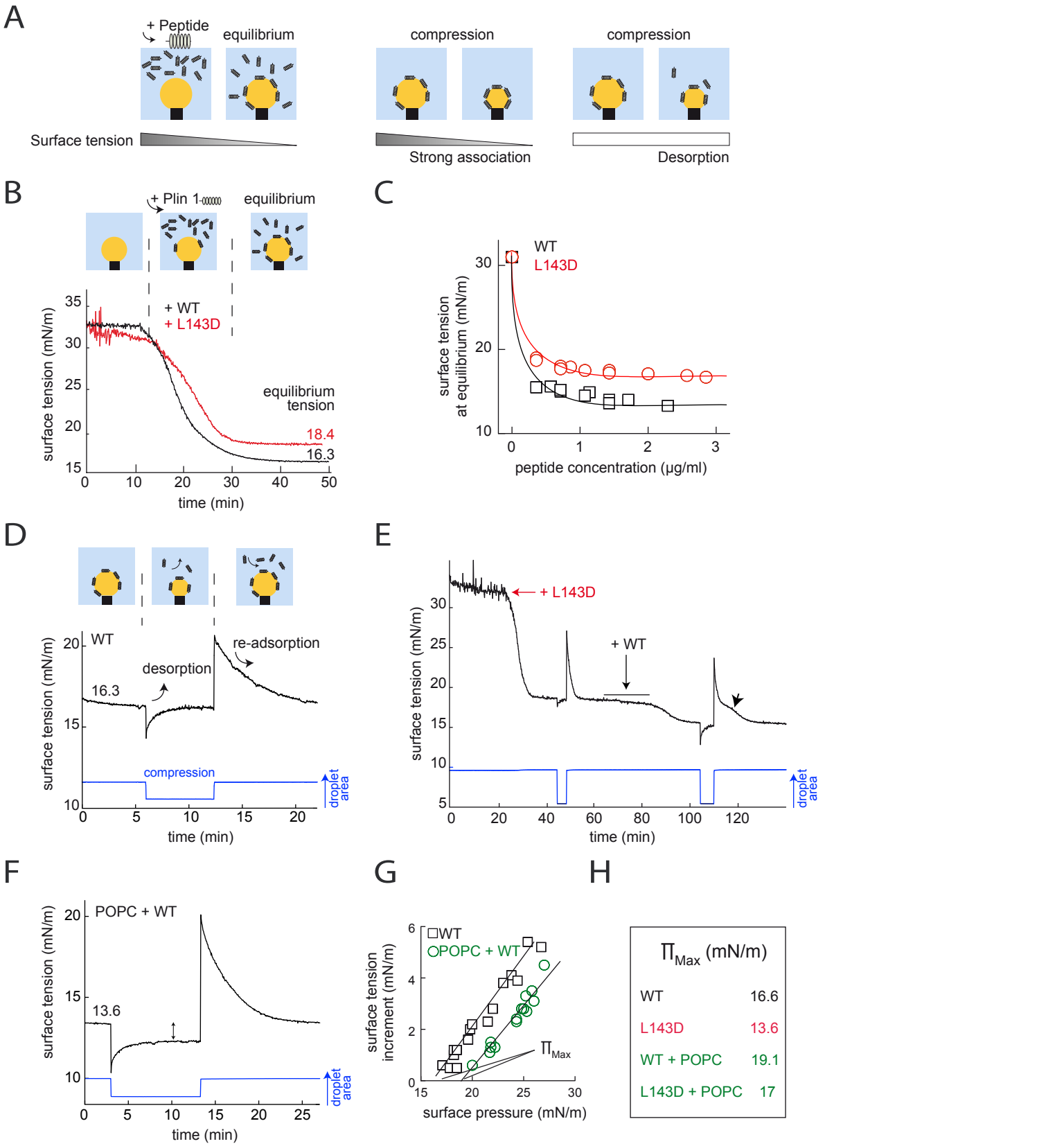
A
+ Peptide
equilibrium
compression
compression
Surface tension
Strong association
Desorption
B
+ Plin 1
equilibrium
+ WT
+ L143D
surface tension (mN/m)
equilibrium tension
18.4
16.3
time (min)
C
WT
L143D
surface tension at equilibrium (mN/m)
peptide concentration (µg/ml)
D
WT
desorption
re-adsorption
16.3
compression
droplet area
surface tension (mN/m)
time (min)
E
+ L143D
+ WT
surface tension (mN/m)
droplet area
time (min)
F
POPC + WT
13.6
surface tension (mN/m)
droplet area
time (min)
G
WT
POPC + WT
Π Max
surface tension increment (mN/m)
surface pressure (mN/m)
H
Π Max (mN/m)
WT 16.6
L143D 13.6
WT + POPC 19.1
L143D + POPC 17

Figure 4

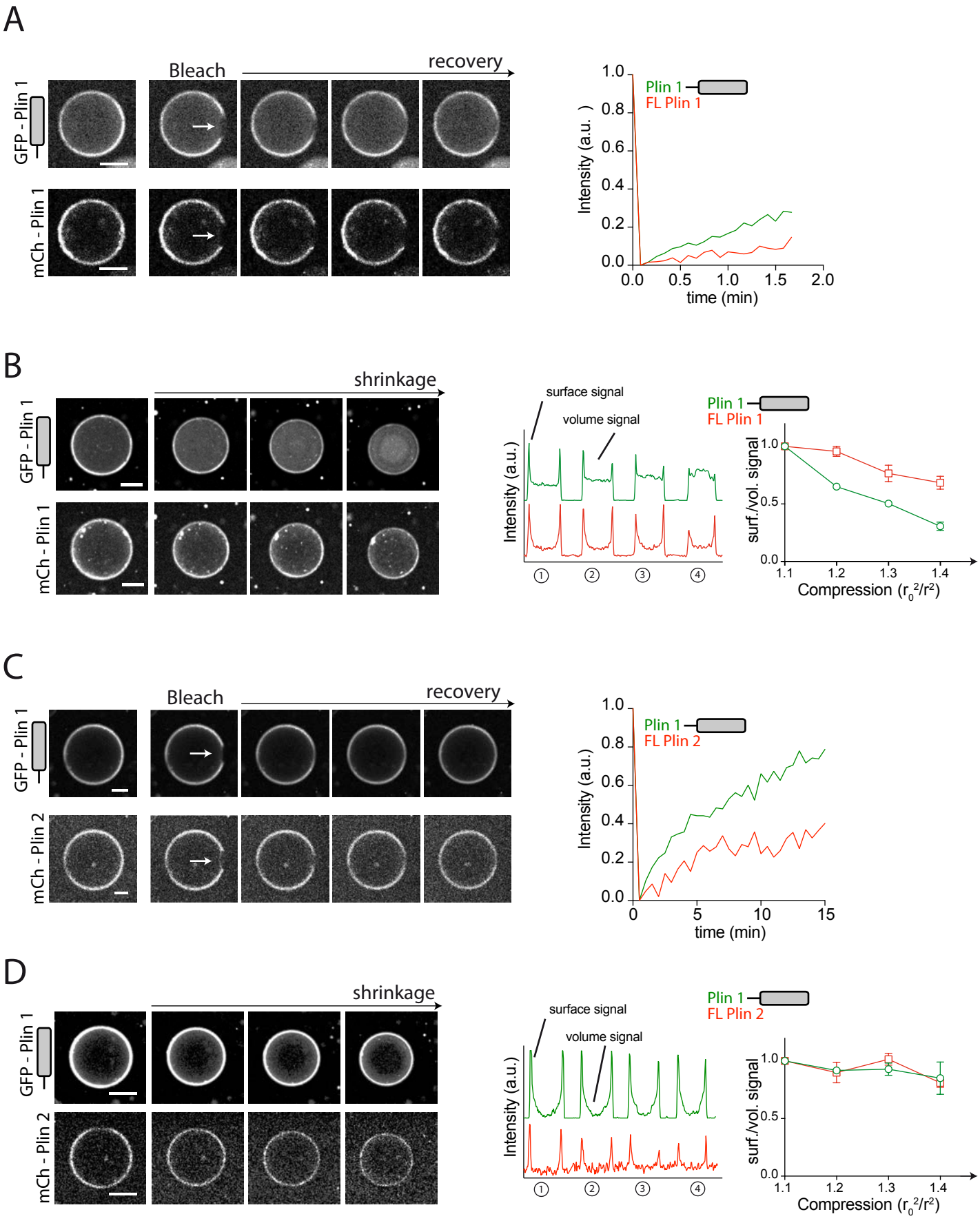
A
Bleach
recovery
GFP - Plin 1
mCh - Plin 1
Intensity (a.u.)
Plin 1
FL Plin 1
time (min)
B
shrinkage
surface signal
volume signal
Intensity (a.u.)
surf./vol. signal
Compression (r0²/r²)
C
Bleach
recovery
mCh - Plin 2
FL Plin 2
D
shrinkage

Figure 4S

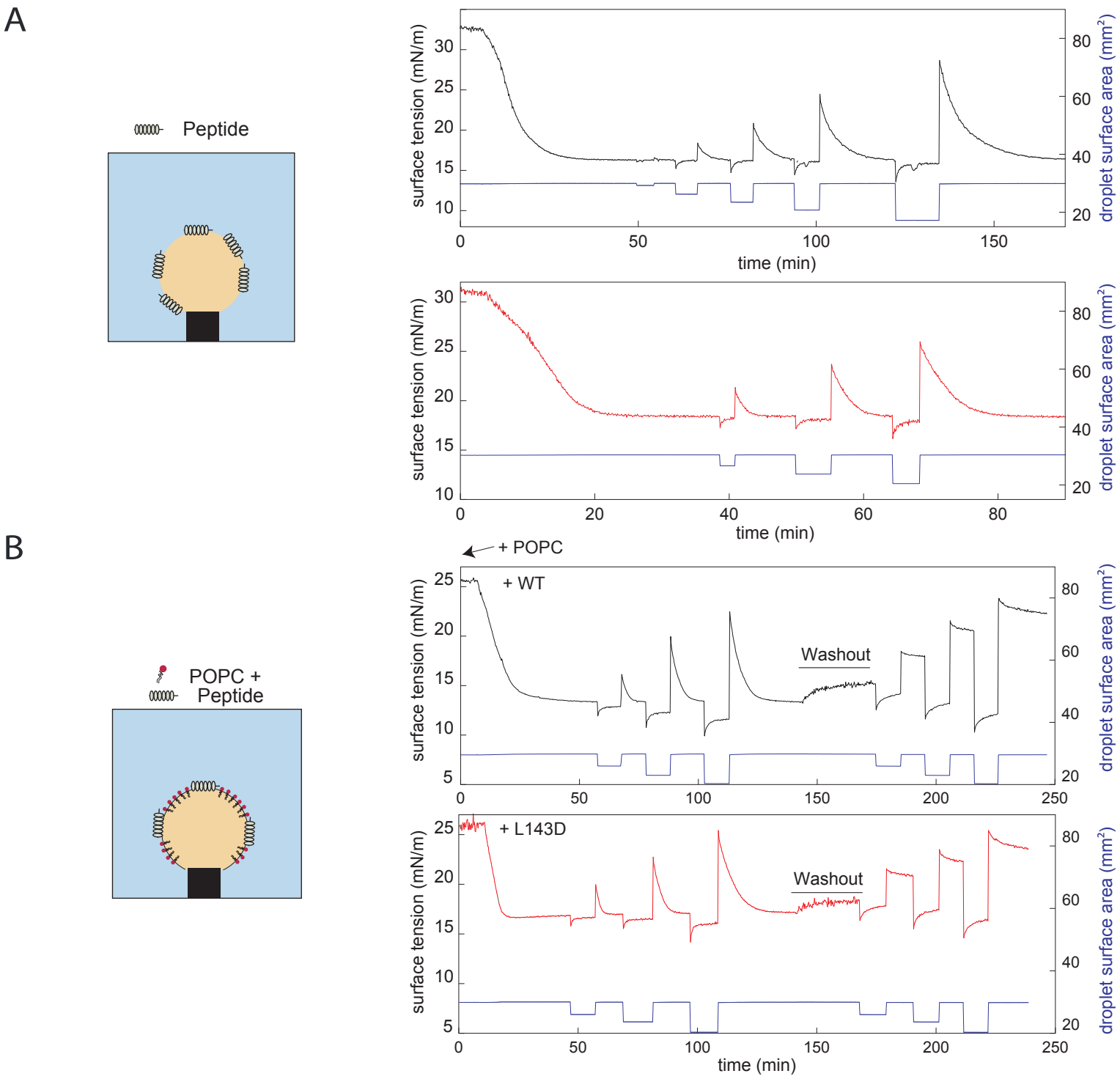
A
Peptide
surface tension (mN/m)
droplet surface area (mm²)
time (min)
B
POPC +
Peptide
+ POPC
+ WT
Washout
+ L143D
Washout
C
+ POPC
+ L143D
+ WT
D
WT
L143D
surface tension increment (mN/m)
surface pressure (mN/m)
POPC + L143D
L143D

Figure 5S